Nano Today 11 (2016) 565–586

Contents lists available at ScienceDirect

Nano Today

journal homepage: www.elsevier.com/locate/nanotoday

Review

Shining carbon dots: Synthesis and biomedical and optoelectronic applications

Fanglong Yuan [a], Shuhua Li [a], Zetan Fan [a], Xiangyue Meng [b], Louzhen Fan [a,*], Shihe Yang [b,*]

[a] Department of Chemistry, Beijing Normal University, Beijing 100875, China
[b] Department of Chemistry, The Hong Kong University of Science and Technology, Clear Water Bay, Kowloon, Hong Kong, China

ARTICLE INFO

Article history:
Received 14 April 2016
Received in revised form 12 July 2016
Accepted 29 August 2016
Available online 21 September 2016

Keywords:
Carbon dots
Bioimaging
Cancer therapy
Light emitting diodes
Solar energy conversion

ABSTRACT

In recent years, the emerging fluorescent carbon dots have shown enormous potentials for biomedical and optoelectronic applications owing to their outstanding characteristics such as good biocompatibility, low cytotoxicity, photostability and versatility in addition to their unique tunable photoluminescence and other exceptional physicochemical properties. In this review, we will update the latest researches on the synthesis, structure, optical and electronic properties of CDs as well as their advanced applications in biomedicine and optoelectronics. We will mainly discuss the applications of CDs in bioimaging with emphasis on stem cells imaging including normal and cancer stem cells, cell nucleus imaging, two-photon fluorescence imaging, red or near-infrared emission for in vivo imaging, cancer therapy including photodynamic therapy, photothermal therapy and chemotherapy, and optoelectronic applications including light emitting diodes and solar energy conversion. Finally, we will size up current challenges on the research of CDs and project future directions of the field. We hope that this review will provide critical insights to inspire new exciting discoveries on CDs from both fundamental and practical standpoints so that the realization of their potential in the biomedical and optoelectronic areas can be facilitated.

Contents

* Corresponding authors.
E-mail addresses: lzfan@bnu.edu.cn (L. Fan), chsyang@ust.hk (S. Yang).

http://dx.doi.org/10.1016/j.nantod.2016.08.006
1748-0132/

Introduction

Since their first discovery in 2006, carbon dots (CDs) as a new family of quantum dots (QDs) have attracted widespread attention and emerged as an excellent fluorescent nanomaterial [1,2]. Literally, CDs are typically a class of zero-dimensional (0D) nanocarbons, or carbon nanoparticles, which are less than 10 nm across with an obvious crystal lattice parameter of ~0.34 nm corresponding to the (002) interlayer spacing of graphite [3,4]. Being prepared in solution, CDs usually possess numerous functional groups such as epoxy, carbonyl, hydroxyl, and carboxyl on their surfaces, which give rise to their high hydrophilicity and readiness for functionalization with various organic, polymeric, or biological species [5]. More importantly, CDs exhibit unique optical properties such as highly tunable photoluminescence (PL) from deep ultraviolet to near-infrared (NIR) and exceptionally efficient multiphoton upconversion, which can be tailored by controlling the size, shape and heteroatom doping of CDs, and by modifying their surfaces and edges, due to the remarkable quantum confinement effect (QCE), surface effect and edge effect [6]. Moreover, compared to organic dyes and traditional semiconductor QDs, not only are CDs advantageous in terms of photostability against photobleaching and blinking, they also have a lower toxicity and better biocompatibility [7,8]. To exploit the unique properties of CDs and their low cost and ease of synthesis, much work has been done in areas such as optical sensing [9–12], bioimaging [13–15], photocatalysis [8,16–18] and electrocatalysis [19–21]. In 2013, highly blue fluorescent CDs were successfully prepared, with a quantum yield (QY ~80%) in aqueous solution comparable to semiconductor QDs, marking a significant advance in this area [22]. Since then, attempts have been made on multiple applications of CDs in biomedicine and optoelectronics such as drug delivery [23], photodynamic therapy (PDT) [24], light emitting diodes (LEDs) [25] and solar cells [26].

As another type of 0D fluorescent carbon nanomaterial, graphene quantum dots (GQDs) have also caught much interest in recent years [27–29]. GQDs are defined as nanographene fragments with a lateral size of less than 10 nm, and as the name suggests, they have a better crystallinity and fewer atomic layers (less than 4, often a single graphene layer) than CDs. GQDs show a characteristic crystal lattice spacing of 0.24 nm, which corresponds to the (100) in-plane lattice parameter of graphene [15,30–32]. A number of review articles have been published on CDs or GQDs separately [3,4,7,8,13,16,33–36]. In the present review, GQDs are included in CDs due to their similar sp^2 carbon structure, elementary composition, photoelectric properties and potential applications. Special attention will be paid to the unique optical properties of GQDs, such as the newly discovered chiral optical properties [37], and their targeted applications for, among others, imaging stem cells [28] or cancer stem cells [38].

In this review, we will survey the latest development on the synthesis, structure, optical and electronic properties of CDs and on their advanced applications in biomedicine and optoelectronics. The latter includes bioimaging with emphasis on stem cell imaging (normal and cancer stem cells), cell nucleus imaging, two-photon fluorescence imaging, red or NIR emission based in vivo imaging, cancer therapy (PDT, photothermal therapy (PTT) and chemotherapy), and optoelectronic applications (LEDs and solar energy conversion), as laid out in Fig. 1. Finally, we call attention to some key opportunities and challenges yet to be addressed for the continual development of CDs. In view of several excellent reviews already appeared in the literature focusing on different aspects of CDs, such as synthesis and optical properties [7,8], biosensing [13,39] and bioimaging [3,9,13], the present review is intended to update the current status of CDs research, provide valuable insights on their functional roles in biomedicine and optoelectronics, and inspire exciting new research directions to accelerate realization of the potential of the intriguing CDs.

Basic chemical and electronic structures of CDs

In general, CDs are 0D nanocarbons with a typical size of less than 10 nm, although ~60 nm size CDs have also been reported [40]. They can be nanocrystallites or amorphous nanoparticles knitted up via sp^2 bonding [41]. The height of CDs ranges from 0.5 to 5 nm depending on the preparation methods. Typical high resolution transmission electron microscopy (HRTEM) images of CDs feature an obvious fringe spacing of 0.34 nm, which corresponds to the (002) interlayer spacing of graphite. On the other hand, GQDs are nanofragments of graphene, and thus have a smaller thickness of less than 2 nm and exhibit a typical fringe spacing of 0.24 nm associated with the (100) in-plane lattice spacing of graphene. Interestingly, after preparation from solution, CDs are indigenously functionalized with complex surface groups, especially oxygen related functional groups, such as carboxyl and hydroxyl, which impart excellent water solubility and suitable chemically reactive groups for surface passivation and derivatization of various organic, polymeric, or biological materials. Oftentimes, these surface groups make great contributions to the optical properties of CDs. For instance, upon surface passivation, the fluorescence properties of CDs are enhanced [42]. Surface functionalization also modifies the physical properties of CDs, with the most obvious example being their solubility in aqueous and non-aqueous solvents. In addition, the large sp^2 π-conjugated structure endows CDs with some excellent characteristics, such as good photostability, high surface area, and robust surface grafting through either π-π stacking or their surface functional groups.

The electronic structure of CDs has been theoretical investigated by several groups. Mandal et al. performed a detailed theoretical calculation to investigate the effect of size, shape and organic functionalization on the electronic structure of CDs [43]. It was revealed that due to the QCE, the highest occupied molecular orbital (HOMO) and the lowest unoccupied molecular orbital (LUMO) of CDs shift to higher and lower energy, respectively, with increasing dot size, thereby reducing the HOMO-LUMO (H-L) gap. Meanwhile, different functional groups (either electron withdrawing or electron donating) strongly modulate the HOMO and LUMO levels, however, no significant change in the H-L gap has been observed. For example, an electron donating group can raise both the HOMO and the

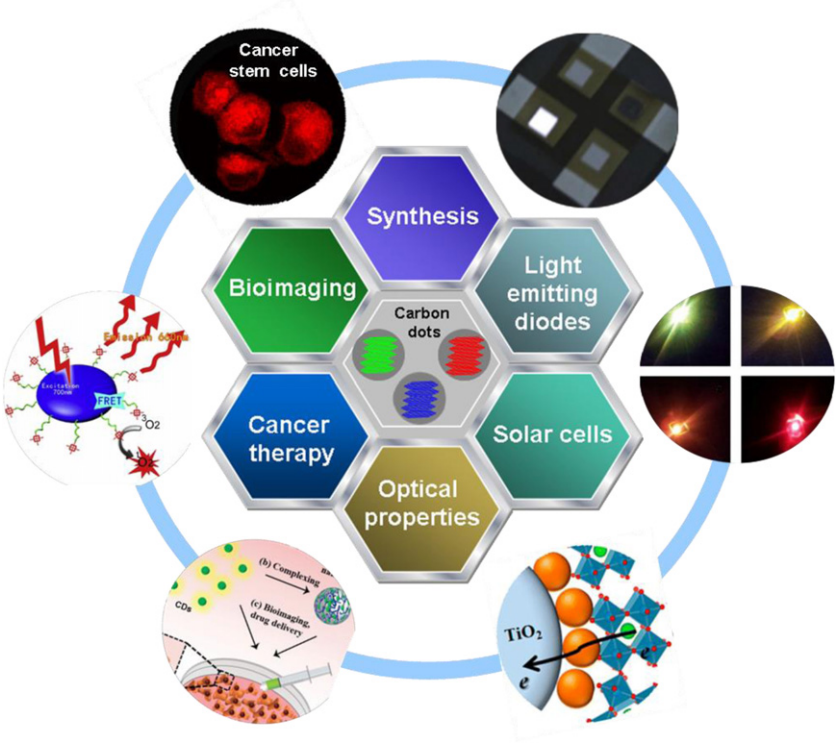

Fig. 1. Schematic illustration of the topical areas of this review, casting the recent trends on applications of CDs in biomedicine and optoelectronics, including bioimaging with emphasis on stem cell imaging, cell nucleus imaging, two-photon fluorescence imaging, red or NIR emission based in vivo imaging, cancer therapy such as PDT, PTT and chemotherapy, and optoelectronic applications in LEDs and solar energy conversion such as solar cells and solar fuels.

LUMO levels to higher energy, while an electron withdrawing group would lower the HOMO and LUMO energies relative to −H passivated CDs. By combining density functional theory (DFT), the GW method and the Bethe-Salpeter equation (BSE), Li et al. found that the electronic structure of CDs is characterized by the competition and cooperation between hybridization of the frontier orbitals with the functional groups and charge transfer therebetween [44]. Functional groups containing a carbon-oxygen double bond (C═O) were demonstrated to be more favorable for tailoring the electronic and optical properties of CDs by introducing a prominent down-shift of the energy levels originated from the π electrons in C═O, which can extend the π-electron system in the CDs. The energy down-shift of LUMO is larger than that of HOMO due to the much larger hybridization of C═O with LUMO than HOMO, which in effect leads to a significant reduction of the energy gap. In contrast, the larger extent of electron transfer from CDs to amino (—NH_2) group than to C═O could result in a larger exciton binding energy and quasi-particle correction in —NH_2 containing CDs than in C═O containing CDs, leading to an enlarged energy gap and partially canceling out the energy gap reduction induced by the hybridization of frontier orbitals with —NH_2 group. Therefore, —NH_2 group can reduce the energy gap of CDs relative to —H passivated CDs, but not as effective as the C═O group. Yamijala et al. have shown that an external electric field can induce a spin-polarized H-L gap in CDs and explained the energy shifts of the molecular orbitals (MOs) under external electric field by plotting electron density difference maps (EDDMs), proving that their results are consistent with the linear Stark effect [45]. Experimentally, Guettinger studied energy levels of CDs in magnetic fields applied perpendicular to the graphene plane and obtained evidence for the formation of Landau levels, where the zeroth Landau level can be used to locate the electron-hole crossover in CDs [46]. At the same time, heteroatoms such as nitrogen, sulfur and other elements were found to significantly alter the structural and physicochemical properties of CDs by tuning the electronic structure. For instance, Li et al. reported a new member of sulphur-doped CDs (S-CDs) prepared by the hydrothermal method using fructose and sulphuric acid as the source materials. The incorporation of ∼1 at% of S into the CDs could effectively modify the electronic structure of S-CDs by introducing S-related energy levels between π and π* orbitals of CDs. The additional energy levels in the S-CDs diversified the electron transition pathways and interband crossing of electrons from the initially excited higher energy levels, giving rise to efficient and multiple emission peaks [47]. This heteroatom doping strategy shows a great potential in optoelectronics and photonics for its simplicity, scalability and low-cost.

Summarizing the above, the unique electronic and chemical structures of CDs can be tuned by their size, shape, surface functional groups and heteroatom doping. Such structural characteristics lend CDs various interesting and useful properties to be discussed below, such as good water solubility, good material stability, high fluorescence efficiency, tunability and stability, non-toxicity, good biocompatibility and easy functionalization. These beneficial properties open up a broad application prospect of CDs in biomedicine and optoelectronics.

Preparation methods of CDs

CDs can be synthesized by two general strategies: top-down and bottom-up methods. The former involves breaking down or cleaving larger carbon structures to smaller ones via chemical, electrochemical, or physical approaches. The latter is realized by pyrolysis or carbonization of small organic molecules or by step-wise chemical fusion of small aromatic molecules. The precursors and synthesis methods chosen often determine the physicochemical properties of the resulting CDs such as the size, crystallinity, oxygen/nitrogen content, fluorescence characteristics including QY, colloidal stability, and compatibility.

Top-down methods

The first reported fluorescent CDs were synthesized by the top-down method through laser ablation of graphite using argon as a carrier gas in the presence of water vapour, followed by acid oxidative treatment and surface passivation [1]. Thereafter, various top-down synthesis approaches towards CDs were developed by reducing the size of graphite, graphene or graphene oxide (GO) sheets, carbon nanotubes (CNTs), carbon fibers, carbon soot and other materials which possess a perfect sp^2 carbon structure and lack an efficient bandgap to give fluorescence. For top-down approaches, many methods have been developed to break down the carbon structure into CDs such as arc discharge [48], laser ablation [1,49], nanolithography by reactive ion etching (RIE) [50,51], electrochemical oxidation [28,29,52–56], hydrothermal [57,58] or solvothermal [6,59], microwave assisted [60,61], sonication-assisted [18], chemical exfoliation [62,63], photo-fenton reaction [64], and nitric acid/sulfuric acid oxidation [27,65–67]. These synthesis methods are invariably complicated and uncontrollable with relative low yields and QY, some even adding hazards to the environment, and thus are not suitable for the large-scale production of CDs with high PL QY.

Bottom-up methods

On the contrary, the bottom-up methods offer exciting opportunities to controlling the CDs with well-defined molecular weight and size, shape and properties by using elaborately designed precursors and preparation processes. Meanwhile, the bottom-up methods are usually low-cost and quite efficient for producing fluorescent CDs on a large-scale, a prerequisite for practical applications of these novel CDs. Laser irradiation of toluene [68], hydrothermal treatment of citric acid [22,69] or carbohydrates [70], stepwise solution chemistry methods using benzene derivatives [20,24,71,72], carbonization of hexaperihexabenzocoronene (HBC) [40] and precursor pyrolysis [73–75] have been utilized to prepare CDs successfully. Apart from the precursors mentioned above, other molecules with abundant hydroxyl, carboxyl and amine groups are also suitable carbon precursors, such as glycerol [76,77], ascorbic acid [78] and amino acid [79], which can dehydrate and further carbonize into CDs at elevated temperatures. Yang et al. reported facile and large-scale synthesis of nitrogen doped CDs with QY of ~80% in aqueous through hydrothermal treatment of citric acid and ethylenediamine, which formed polymer-like CDs first and then carbonized into CDs [22]. Moreover, the emission color and QY of CDs can be effectively tuned by adjusting the ratio of reagents or the amount of ancillary inorganic substrate (e.g. H_3PO_4, KH_2PO_4, NaOH). For instance, Bhunia et al. synthesized highly fluorescent CDs with tunable visible emission from blue to red on gram-scale from different kinds of carbohydrates and dehydrating agent (H_3PO_4, H_2SO_4) at various temperatures [80]. The dehydrating agents and the reaction temperature were varied to control the nucleation and growth kinetics. This synthetic method could restrict the particle size to smaller than 10 nm and afford an appropriate chemical composition of CDs for tunable emission with a relative high fluorescence QY.

Optical properties of CDs

Despite the diverse structures of CDs prepared from different approaches with different precursors, CDs usually share some similar optical properties in terms of absorption and fluorescence characteristics. In this section, the common optical properties of CDs that have been revealed are briefly summarized.

UV–vis absorption

CDs are an effective photon-harvester in the short-wavelength region due to light absorption by the π-conjugated electrons in a sp^2 atomic framework. Typically, they show strong optical absorption in the UV region (230–320 nm), with a tail extending into the visible region. The broad peak at ~230 nm can be ascribed to the π-π* transition of aromatic C=C bonds, whereas a shoulder at 300 nm is attributed to the n-π* transition of C=O bonds or other connected groups [28,63,65]. The difference in size, composition or structure of the hybridization derivatives such as the functional groups and surface passivation can also alter the absorption characteristics of CDs.

Photoluminescence

One of the most fascinating features of CDs, from both the mechanistic and practical standpoint, is their tunable PL properties stemming from the QCE and edge or surface effects of their large rigid conjugated structure. Differently colored CDs have been synthesized with different approaches, ranging from deep ultraviolet to red or even NIR emission and most commonly blue and green [24,81]. In general, the PL spectra of CDs are almost symmetrical on the whole wavelength scale. The fluorescence spectra are usually broad due largely to the wide dot size distribution, and exhibit large Stokes shifts compared with semiconductor QDs and organic dyes, due to the diverse electronic transition pathways. The peak of CDs usually show excitation-dependent behavior, that is, the emission peak can vary contingent on the excitation wavelength, which may result from the wide size distribution of CDs, a variety of surface defect-states or different emissive traps [82]. Notwithstanding, the excitation-dependent PL behaviors of CDs are highly promising for multicolor imaging applications [41,83].

The QY of CDs varies with the fabrication method and the surface chemistry involved. For unpassivated CDs, the QY is always relatively low because the electron withdrawing groups of carboxylic (—COOH) and epoxy groups can act as non-radiative electron-hole recombination centers on the surface and decrease the π electron cloud density of CDs [84]. Therefore, after surface modification or passivation by transforming the —COOH and epoxy groups of CDs into —CONHR and —CNHR with amino-group containing molecules, such as ammonia, alkylamine and anilines, or polymeric molecules, such as polyethyleneimine and amine-terminated oligomeric polyethylene glycol, the QY can be dramatically increased, attributable to the reduction of the non-radiative recombination induced by the —COOH and epoxy groups [61,85,86]. Moreover, the passivation with strong electron donating functional groups such as —CONHR and —CNHR can greatly increase the π electron cloud density of CDs and facilitate the radiative recombination of confined electrons and holes in quantum-sized CDs, which can also improve the QY of CDs [87]. Doping CDs with heteroatoms could also effectively modulate their bandgap and electronic density, enhancing chemical activity and QY of CDs for practical applications, which were demonstrated through theoretical calculations and detailed experiments [12,20,52]. The QY of CDs have been continually improved along the way, with the highest of ~80% in aqueous solutions reached by blue fluorescent CDs after nitrogen doping [22]. However, the QY of other color fluorescent CDs is mostly less than 20%, much lower than traditional semiconductor QDs and organic dyes. Compared to CDs, GQDs usually have an even lower QY with the highest reported so far being about 54.5% for blue fluorescence emissions [75]. The relatively low QY of CDs for longer wavelength emissions beyond the blue light region may arise from the too many variegated defects of CDs prepared with the currently available methods, which often prevent efficient passivation and amellioration. Therefore, it remains a challenge to develop facile and efficient approaches for controllable synthesis of well-defined high quality CDs on a large-scale with a much higher PL QY comparable to semiconductor QDs especially in the long wave-

length region, which has so far hindered most of the applications of CDs.

In addition to the conventional down-conversion fluorescence emissions, certain CDs are also found to display up-conversion fluorescence emissions (anti-Stokes PL), which are orders of magnitude higher in efficiency than conventional fluorophores [6,88–90]. Up-conversion fluorescence emission is an optical phenomenon wherein the fluorescence emission wavelength is shorter than the excitation wavelength. This is particularly attractive for in vivo imaging due to the deep-tissue penetration ability of long excitation wavelengths especially in the NIR region, and for molecular imaging with high spatial-resolution, low back ground interference, and low photon-induced toxicity because of the highly-localized nonlinear photon adsorption process. However, it should be pointed out that some of the apparent up-conversion fluorescence emissions of CDs reported might be artefact. Gan et al. revisited several publications that reported the up-conversion PL in CDs under excitation from a xenon lamp. Experiments have revealed that the PL was an artificial up-conversion emission, which was essentially excited by the second-order diffraction light of wavelength $\lambda/2$ coexisting with the excitation light of wavelength λ in the light source. By simply inserting a long pass filter into the excitation pathway, the so called up-conversion PL could not be detected. Therefore, great cautions are required to interpret the up-conversion fluorescence emissions of CDs and further clarifications are often necessary. The real up-conversion from CDs can be excited under a high enough power density from a femtosecond pulsed laser [91]. So it is of great importance to establish a proper characterization system before one can truthfully investigate the up-conversion PL properties of CDs, which do offer a great potential as well for biomedical and optoelectronic applications.

Photostability is a key property for fluorescent materials to be used in the biomedical field. Organic dyes have been widely used in the biomedical field but often suffer from the serious photobleaching problem. Similarly, photo-blinking of semiconductor QDs also goes against the biomedical applications. On the contrary, CDs prepared by different methods usually possess non-blinking PL and excellent photostability due to the large rigid π-conjugated structure system after surface passivation. These merits have not only enabled single-molecule tracking but also permitted long-term real-time imaging for biomedical applications. Scanning confocal microscopy study showed that neither blinking nor significant PL intensity decay of CDs were observed during several hours of continuous exposure to excitation light [1]. The PL intensity of CDs prepared by laser ablation decreases by only 4.5% after 4 h of irradiation, whereas organic fluorophores photobleach within minutes [92]. No distinct photobleaching was observed for CDs prepared from solvothermal method using hand-held UV lamp or mercury (Hg) lamp with a low power, and only when using a 1000 W high pressure Hg lamp did the PL intensity decrease [93].

Chiroptical properties

Chirality is one of the most important optical properties of a material. There are many natural processes wherein chiral compounds play a major role, such as molecular recognition, chemical reactions, biological metabolism and medical intervention. Therefore, an understanding of the fundamental concepts relevant to chirality in nanostructures is important for the further advancement of nanoscience and nanotechnology [94].

Chirality of graphene-based materials such as graphene nanoribbons has been observed on single pieces with the help of atom probe microscopy [95]. Plasmonic effects in single or a few layered graphene sheets coupled with exciton confinement in quantum-sized GQDs make it interesting to introduce chirality to this material. The chiral GQDs and potentially other forms of graphene sheets with nanoscale chirality can be obtained by leveraging intermolecular interactions of surface functionalized chiral organic ligands and the attendant out-of-plane buckling of the graphene sheets. Studies of chiral GQDs will contribute to the understanding of chiroptical phenomena in delocalized states and their utilization in biomedicine and polarization-based optoelectronics.

Until very recently in 2016, the chirality of GQDs was first reported by Nakagawa et al. The chiral GQDs (CGQDs) was synthesized by covalent functionalization of GQDs with enantiomerically pure (R) or (*S*)-2-phenyl-1-propanol (Fig. 2a_1) [37]. They demonstrated the concept that GQDs could become chiral after covalent functionalization with chiral organic ligands and this chiroptical property could be transferred to a supramolecular structure built with pyrene molecules, where the CGQDs/pyrene ensembles showed a characteristic chiroptical response depending on the configuration of the chiral organic ligands introduced (Fig. 2a_2). Based on this simple approach, it is possible to construct more sophisticated chiral carbon-based GQDs supramolecular organizations where chirality could play an important role in practical application. Almost at the same time, Suzuki et al. reported the asymmetric synthesis of CGQDs by covalent edge modification with L- and D-cysteine, leading to the nanoscale twist of the flexible graphene sheets (Fig. 2b_1) [96]. Quantum mechanical chiral induction occurs at the edges of the GQDs due to hybridization of MOs of the edge ligands and those of peripheral carbon atoms. The resulting L- and D-GQDs represent an example of symmetry-related carbon nanostructures with nearly mirror image optical activity (Fig. 2b_2). The high-energy chiroptical peaks at 210–220 nm correspond to the hybridized MOs involving the chiral center of amino acids and atoms of graphene edges. Diverse experimental and modeling data, including DFT calculations of CD spectra with probabilistic distribution of GQDs isomers, indicate that the newly formed band at 250–265 nm originates from the three-dimensional twisting of the graphene sheet and can be attributed to the chiral excitonic transitions (Fig. 2b_3).

PL mechanism of CDs

Although the optical properties of CDs have been extensively studied with great progress in recent years, the mechanisms underlying the tunable PL properties are still a most controversial issue, mainly due to inconsistent experimental observations caused by the large heterogeneity of CDs samples even from the same synthesis, as well as the multifarious, obscure and poorly defined properties of CDs obtained from different preparation processes. For example, the anticipated size-dependent emission of ideal CDs has not been unambiguously demonstrated by experiments [97]. Experimental determination of the PL mechanisms hinges upon effective approaches to controllably synthesizing well-defined CDs, which are deadly lacking. It has been suggested that graphene pieces of any size will show remarkable QCE due to the infinite Bohr diameter of excitons in graphene. As a result, CDs have a non-zero bandgap and the associated PL, which can be tuned by altering the size and surface chemistry of CDs [98].

Although great progress in the preparation of CDs has been made in the last five years, the exact origins of the fluorescence emissions remain debatable and much more research is urgently needed to paint a clearer mechanistic picture of the fluorescence emissions. Two popular PL emission models have been proposed for CDs: one is based on the bandgap transitions in conjugated π-domains, where the QCE features prominently, while the other is related to surface defect-states, which primarily manifest the edge effect.

Bandgap transitions of conjugated π-domains

A major trait of QDs is the QCE, which occurs when QDs are smaller than their exciton Bohr radius. For CDs made of a perfect

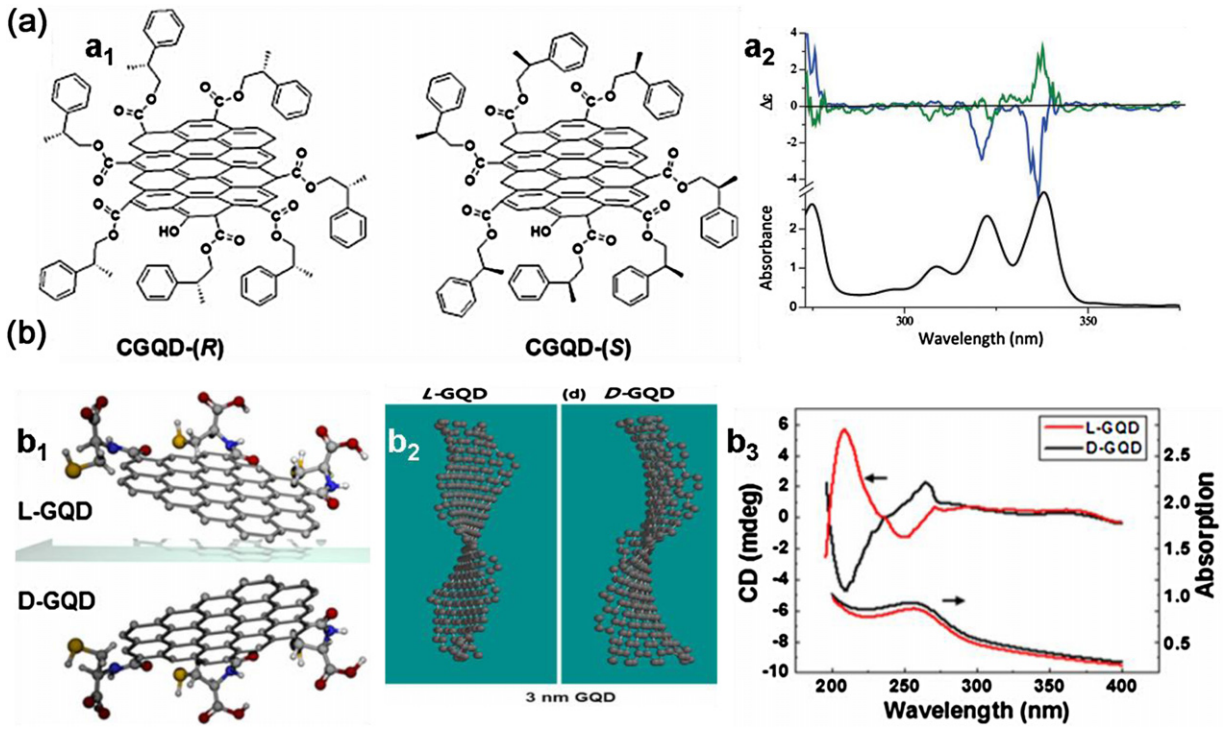

Fig. 2. (a_1) CGQDs obtained from esterification reaction with enantiomerically pure alcohols, (a_2) Top: CD spectra in NMP for aggregates CGQDs-(R)/pyrene (blue) and CGQDs-(S)/pyrene (green). Bottom: UV-vis spectrum of pyrene in NMP. Reprinted with permission from [37]. Copyright 2016 Royal Society of Chemistry. (b_1) Schematic structures of a pair of enantiomeric CGQDs, (b_2) Optimized geometry of a graphene sheet in model GQDs viewed from the direction of the largest dihedral angle, (b_3) CD spectra for L-GQDs (red) and D-GQDs (black) dispersions. Reprinted with permission from [96]. Copyright 2016 American Chemical Society.

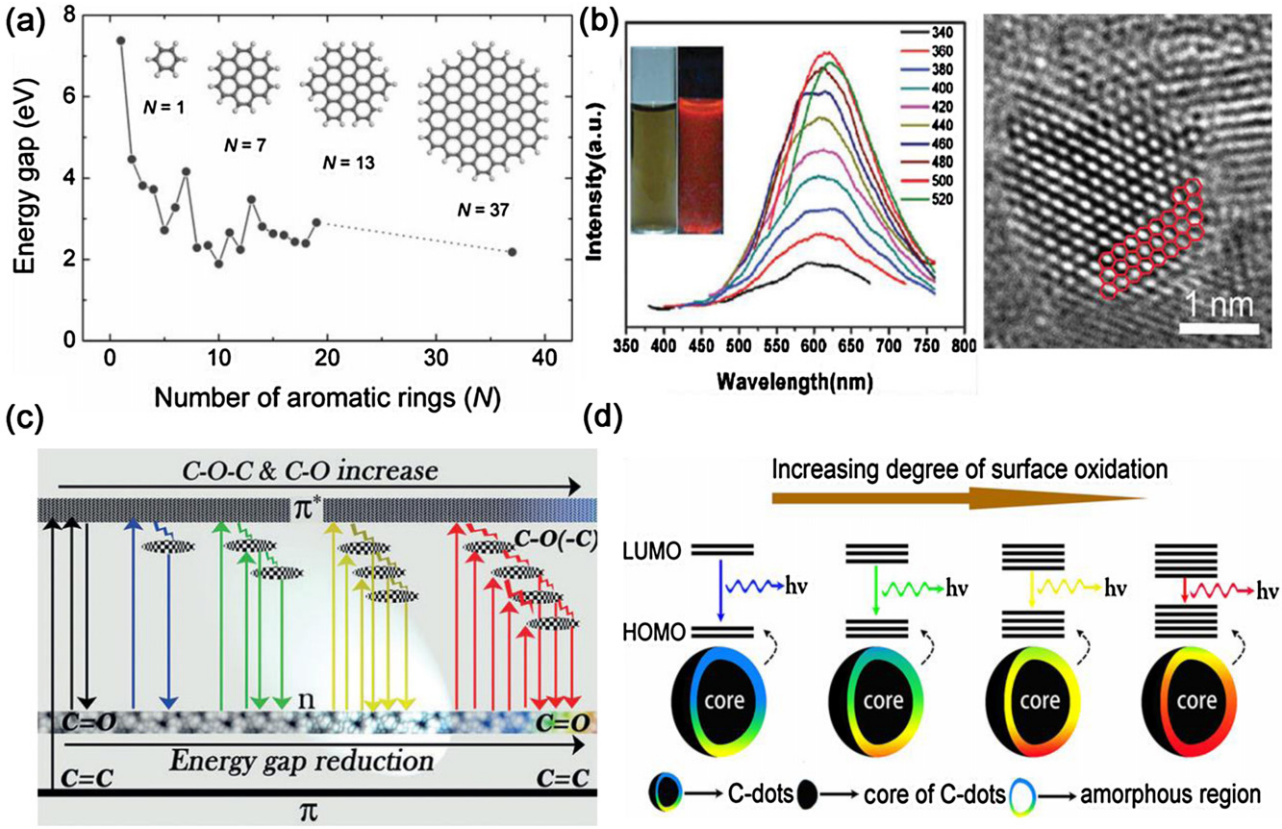

Fig. 3. (a) Energy gap of π-π* transitions calculated using DFT as a function of the number of fused aromatic rings. Reprinted with permission from [99]. Copyright 2010 John Wiley and Sons. (b) PL spectra and sp^2 domains of RF-GQDs. Reprinted with permission from [29]. Copyright 2015 Royal Society of Chemistry. (c) Illustration of the tunable PL emission from CDs containing different O-related surface groups. Reprinted with permission from [110]. Copyright 2015 John Wiley and Sons. (d) Model for the tunable PL of CDs with different degrees of oxidation. Reprinted with permission from [111]. Copyright 2016 American Chemical Society.

graphene fragment with few surface chemical groups, the bandgap of conjugated π-domains is thought to be the intrinsic PL center. Theoretical modelling and calculations allow precise isolation of the influence of the size on the PL of CDs. DFT calculations have clearly shown that the bandgap increases from approximately 2 eV for CDs consisting of 20 aromatic rings to 7 eV for benzene (Fig. 3a) [99]. Using DFT and time-dependent DFT calculations, Sk et al. also concluded that PL of CDs essentially originates from the QCE of conjugated π- electrons in sp^2 carbon network, and can be sensitively tuned by their size, edge configuration and shape. Typically, zigzag-edged pristine CDs emit from deep UV to near infrared depending on the diameter of CDs, as the π-electron delocalization tends to lower the bandgap by virtue of the QCE [100]. Moreover, zigzag-edged CDs exhibit distinct quantum confinement properties compared with armchair-edged CDs. Contrary to the armchair-edged counterparts of CDs, the localized states at zigzag edge sites lower the energy of the conduction band and thus reduce the bandgap. Thus, it is expected that the similarly-sized CDs with an armchair edge would widen the bandgap and consequently blue-shift the emission.

Our group successfully prepared water-soluble, 3 nm uniform-sized red fluorescent GQDs (RF-GQDs) with no chemical modification by direct electrochemical exfoliation of graphite in a $K_2S_2O_8$ solution (Fig. 3b) [29]. We identified isolated sp^2 domains with a diameter of about 3 nm, and the very active $SO_4^{\bullet -}$ radicals produced from $S_2O_8^{2-}$ acted as electrochemical "scissors" to sharply cut the graphene sheets into small intact sp^2 structures, known as the RF-GQDs we obtained. To the best of our knowledge, this is the first report on the direct observation of "molecular" sp^2 domains with a diameter of about 3 nm that is directly responsible for the red emission. The size-dependent QCE of CDs has been observed by several groups [101]. Kang et al. separated the CDs prepared from electrochemical method via column chromatography to obtain samples with different sizes ranging from 1.5 to 3 nm, and the blue, green, yellow and red PL was strong enough to be seen with the naked eyes. Meanwhile, the relationship between the PL and CDs size obtained from theoretical calculations agreed well with the optical measurement results [102]. Liu et al. synthesized highly homogeneous blue fluorescent CDs with a pure sp^2 carbon crystalline structure and few oxygenous defects by chemically exfoliating graphite nanoparticles, providing an ideal platform for in-depth studies on the PL origin of nanosized graphene. CDs show a significant absorption peak at 275 nm, which coincides well with the PLE peak and is thus indicative of the intrinsic state in CDs. Moreover, the optimized excitation in the short wavelength region and the fast radiative recombination support the conclusion that the blue emission originates from the intrinsic states [62]. More recently, Lin et al. synthesized fluorescent CDs with three primary colors of blue, green and red emissions corresponding to average sizes of about 6.0, 8.2, and 10 nm by solvothermal treatment of phenylenediamine [103]. The highest QY of red fluorescent CDs reached ~26% in an ethanol solution, which was ascribed to the high nitrogen content of 15.5 at%. Of note, the sizes of differently colored CDs appear to be inconsistent with some other reports or the theoretical calculation results [99,100]. Here it should be emphasized that it is the size of the sp^2 domains rather than the size of the nanoparticles per se that dictates the emission color of CDs. Most reported CDs are actually made of isolated sp^2 domains dispersed within a sp^3 matrix due to the want of efficient methods for the controllable synthesis of wholly perfect sp^2 structured CDs.

Surface defect-states

The second kind of the fluorescence mechanism of CDs arises from surface-related defect states. Both sp^3 and sp^2 hybridized carbons and other surface defects of CDs [86,88], such as oxygen containing functional groups, contribute to the multicolor emissions of CDs from their localized electronic states [104,105]. It has been reported that surface defects, which are primarily created through surface oxidation, can serve as capture centers for excitons, thus giving rise to surface-related defect state fluorescence [106]. A higher degree of oxidation on the CDs surfaces implies more surface defects and introduces more emission sites, resulting in a more red-shifted emission [107]. Another report by Chen et al. proposed, with support from DFT calculations, that the carboxyl groups on sp^2-hybridized carbons could induce significant local distortions and consequently narrow the energy gap [108]. Reduction of these oxygen containing functional groups may completely change the optical properties and give rise to radically different PL wavelength and intensity distributions [89,109]. Hu et al. produced a series of CDs by varying the reagents and reaction conditions and concluded that the surface epoxides or hydroxyls were predominantly responsible for the resulting PL red shift (Fig. 3c) [110]. More recently, Ding et al. also observed red shift of the emission peaks of CDs from 440 to 625 nm, which was ascribed to a gradual reduction of bandgap with increasing incorporation of oxygen species into the surface functional groups (Fig. 3d) [111]. The oxygen containing functional group-related defect state emission of CDs has also displayed pH dependent behavior. The fluorescence intensity and even the emission peak wavelength of CDs always change significantly with the pH of a solution, which may result from the electrostatic doping/charging of the CDs and the corresponding shifting of Fermi level due to the deprotonation or protonation of the oxygen containing functional groups [78,112–114]. Our group have synthesized a new type of water-soluble, multicolor fluorescent GQDs, which can be responsive to all-pH from 1 to 14 and observed with the naked eye. For the first time we demonstrated the novel surface molecule state of red emission of quinone structures transformed from the lactone structures in strong alkaline conditions [27]. The pH-dependent PL is very important for investigating the fluorescence mechanisms of CDs, the understanding of which is still at an early stage and more in-depth studies are still required to address this issue.

In addition to oxygen-containing groups, amine-containing groups also contribute to the surface states in CDs. Tetsuka et al. reported an ammonia-assisted hydrothermal method for the preparation of CDs, which was edge-terminated by a primary amine, allowing the electronic structure to be modified by the effective orbital resonance of the amine moieties and the graphene core [59]. The emission peak red shifted with increasing numbers of amine groups for CDs of the same size. The resonance feature between the orbital localized in the $-NH_2$ groups and the delocalized π orbital of CDs results in a narrowing of the optical bandgap. In addition, such a resonance orbital can lead to the process of intersystem crossing emission as a result of enhanced spin-orbital coupling. Such amino-containing CDs have also been reported by other groups. Jin et al. demonstrated that both DFT calculations and experiments proved the decrease of bandgap by tuning the concentration of modified amino groups [115]. Kumar et al. also investigated the PL behaviors of amino-functionalized CDs. First-principles calculations suggested that primary amine moieties resulted in the formation of an additional inter-band level at about 3.28 eV relative to the reference position of Fermi level within the energy gap owing to *p*-orbital hybridization of C—N atoms at the edge sites [116]. Variations in surface state and nitrogen content have also been found to be effective for preparing CDs with tunable fluorescence. Through hydrothermal treatment of different precursors such as well defined polythiophene derivatives, multicolor fluorescent CDs with tunable emissions ranging from blue to NIR region at a single excitation wavelength (400 nm) were successfully prepared. The PL tenability was shown to be dependent on the surface states and nitrogen content [117].

Interestingly, the surface defect-state emissions and bandgap emissions of π-conjugated domains can both be found in individual CDs. Pang et al. prepared a series of CDs by altering the reaction conditions and ascribed the PL red shift to both quantum size effects and surface states [106]. The energy gap was demonstrated to be correlated with the extent of π-conjugation and the surface chemical functional groups of CDs. Wang et al. found that a dark intrinsic state (bandgap transitions of π-conjugated domains) and two independent molecule-like states (surface defect-states) existed in CDs synthesized by solvothermal method [118]. The intrinsic state is attributed to the graphene core and its PL centers at about 470 nm. Two independent molecule-like states exhibited blue and green fluorescence, with emission peaks at about 430 and 530 nm, respectively. Seo et al. also revealed that the green luminescence originates from defect states with oxygenous functional groups, whereas the blue luminescence is dominated by intrinsic states in the highly crystalline structure of CDs [62]. By time-resolved PL spectroscopy, Vanthan et al. showed two different pathways of electron-hole radiative recombination in CDs with distinct relaxation time scales: a slow relaxation of carriers from the carbogenic core (about 14 ns) and a fast decay by direct radiative recombination of carriers on the surface states (about 1.3 ns) [49]. It was found that the surface defect-state emission can be removed through surface modification of the CDs. For instance, after the transformation of —COOH and epoxy of CDs into —CONHR and —CNHR with alkylamines, the intrinsic-state blue emission was greatly enhanced while the surface defect-state green emission disappeared [89].

Although some progresses regarding the PL mechanisms of model CDs have been achieved, it is still not very clear about how the PL is influenced by the numerous complicated factors in an individual CDs, such as size, shape, crystallinity, defects, functional groups, surface functionalization and heteroatoms doping. Both in-depth experimental verifications and theoretical calculations are still urgently needed to provide convincing explanations for the PL mechanisms. One of the most important challenges to address this issue is to develop an efficient method for large-scale production of high quality CDs with a well-defined structure. The CDs reported thus far usually show different sizes and different crystallinity, uncertain surface defects and functional groups, making it difficult to determine the factors that control the PL emissions. Once the chemical structure of CDs can be well controlled in the preparation process, it will be possible to clinch on the PL mechanisms of CDs. Meanwhile, the study of CDs prepared with different precursors and by different methods in a systematic fashion will also be very helpful to sort out the factors that dominate the PL mechanisms of CDs.

Electronic properties of CDs

Besides the rich optical properties described above, CDs also have several excellent electronic properties due to the special QCE and edge effects, some of which have already been uncovered. For example, the PL from CDs can be quenched efficiently by either electron acceptor or electron donor molecules in solution, namely, photoexcited CDs are either excellent electron donors or electron acceptors. These interesting photoinduced electron transfer properties should offer new opportunities to use CDs for light energy conversion and related applications [119,120]. Williams et al. detected ultrafast electron injection from photoexcited CDs to the TiO_2 conduction band with a time constant $\tau_i < 15$ fs and charge recombination dynamics characterized by a fast channel ($\tau_{r1} = 80–130$ fs) and a slow one ($\tau_{r2} = 0.5–2$ ps) [121]. They further discussed the feasibilities of implementing the hot carrier solar cell using CDs. Our group have demonstrated that the GQDs could act as a superfast electron tunnel between the photoexcited perovskite and the electron transporting TiO_2, resulting in a significant power conversion efficiency improvement of perovskite solar cells [26]. Li et al. first studied the electronic energy relaxation pathways in uniformly sized CDs and found that the photoexcited CDs had a significant probability of relaxing into triplet states and emitted both fluorescence and phosphorescence at room temperature with relative intensities depending on the excitation energy. Due to the long lifetime and the reactivity of triplet electronic states, the results could have significant implications for applications of CDs [122]. Before long, they discovered that the carrier cooling in CDs could be two orders of magnitude slower than those in bulk graphene materials with hot-electron lifetimes as long as hundreds of picoseconds, which could enable the harvesting of hot charge carriers to improve the efficiency of solar energy conversion [123].

Biomedical applications of CDs

With the unique optical properties, the large surface area and the amenability to surface functionalization, CDs have shown great potential for a variety of biomedical applications. Meanwhile, biosafety concerns about CDs have gradually come to the fore as their possible industrial and biomedical applications become more and more apparent. Till now, no acute toxicity or morphological changes have been found from in vitro cytotoxicity studies of CDs using a series of cell lines [124,125]. More recently, in vivo studies have also indicated the low toxicity and good biocompatibility of CDs [126,127]. Neither severe symptoms of inflammation were observed in the liver, kidney, spleen, heart, or lung in rats as evidenced by blood biochemistry and hematological analysis. These findings are encouraging, providing substantial evidence for the safety of CDs in biomedical application. A large body of work has shown that CDs offer robust platforms for cellular imaging, in vivo imaging, cancer diagnosis and therapy.

Bioimaging applications of CDs

CDs are superior to the current organic dyes and semiconductor QDs due to their stable PL, low cytotoxicity and good biocompatibility. These merits make CDs desirable alternatives to probe biological systems both in vitro and in vivo. Considering that several reviews have focused on the cancer cell imaging [13–15], here we will mainly bring up to date the status of the exciting CDs-based bioimaging area, especially on in vitro imaging, including stem cell imaging, cell nucleus imaging and two-photon fluorescence imaging, and in vivo imaging.

Stem cell imaging

Stem cells give rise to tissue progenitor cells and in turn differentiate into tissue-forming cells, which are central to the understanding of the native development and tissue regeneration [128,129]. When stem cells or their progeny regenerate tissues and organs, there is a critical need to delineate the relative contribution to the regenerated tissues and organs from delivered cells versus host cell. Thus long-term and cytocompatible labeling of stem cells is critically needed in the field of regeneration medicine for understanding their fate, migration and contribution to the regenerating tissues. Although CDs can penetrate into the cancer cells effortlessly for imaging in various studies [27,52,103,125,130–133], stem cells labeling still poses a considerable challenge due to their particularity. Our group firstly used stabilizer-free GQDs as a fluorescent labeling agent in long term stem cell imaging [28]. Bright yellow fluorescent GQDs with 14% QY have demonstrated direct and easy penetration into three different kinds of stem cells, neurospheres cells (NSCs), pancreas progenitor cells (PPCs) and cardiac progenitor cells (CPCs) without affecting their viability, proliferation or differentiation capacity. As shown in the confocal fluorescent

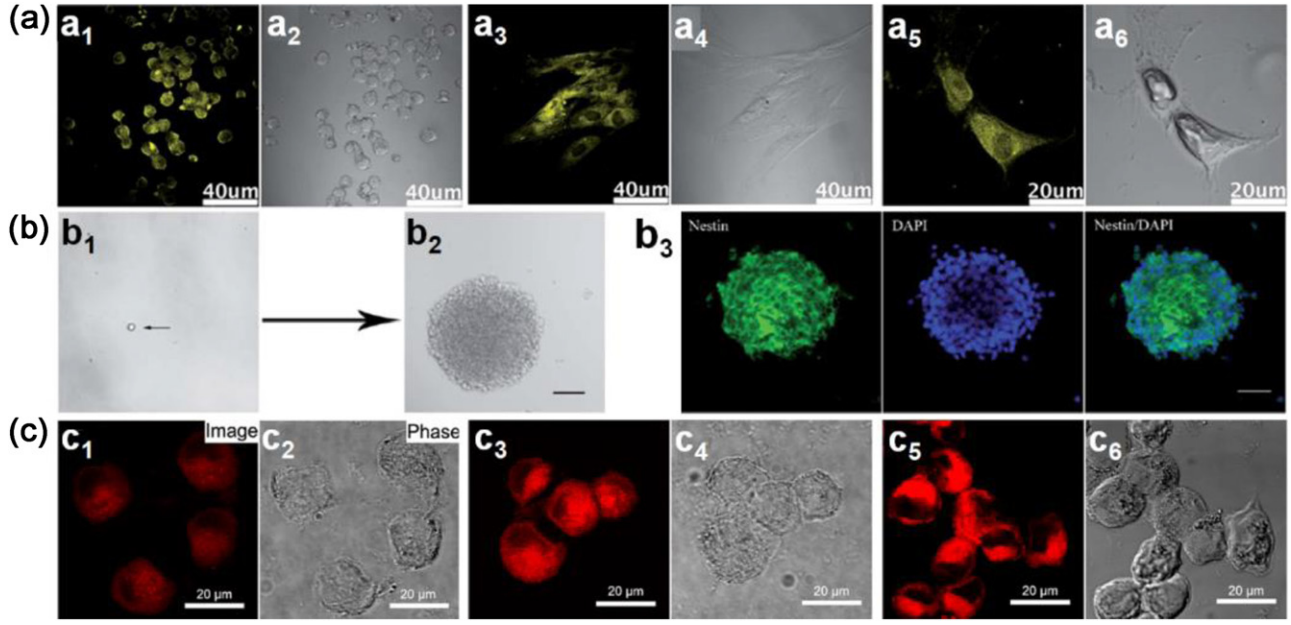

Fig. 4. Confocal fluorescence microscopy images of stem cells of NSCs (a_1), PPCs (a_3) and CPCs (a_5) incorporated with the fluorescent GQDs and corresponding images under bright field (a_2, a_4, a_6). Reprinted with permission from [28]. Copyright 2012 Royal Society of Chemistry. (b) Images showing that GQDs do not spoil the self-renewal ability and expression of the cell type-specific marker in hNSCs. The GQD-labeled hNSCs were dissociated into single cell (b_1), as shown with the black arrow and the single cell formed large neurospheres (b_2) after 12 days. (b_3) Immunofluorescent staining for nestin protein in the neurospheres showed nestin-positive cells (green). Nuclei are stained with DAPI (blue). Reprinted with permission from [134]. Copyright 2014 Royal Society of Chemistry. (c) Confocal fluorescence microscopy images of pancreatic CSCs incubated with 10 μM, 25 μM, and 50 μM Fe^{3+} for 5 h, respectively, followed by further incubation with RBD-GQDs (25 mg/L) for 0.5 h. Reprinted with permission from [38]. Copyright 2015 American Chemical Society.

images (Fig. 4a), the morphology of stem cells could be clearly discerned after incubated with GQDs. We further investigated the uptake mechanism and biocompatibilty of such GQDs with human neural stem cells (hNSCs) [134]. TEM images confirmed that the GQDs were indeed internalized by the hNSCs via the endocytosis mechanism and were located in the cytoplasm. And GQDs did not affect the self-renewal and expression of the cell type-specific marker in hNSCs. The single cell dissociated from GQDs-labeled hNSCs formed large neurospheres after 12 days in normal culture medium (Fig. 4b_1) and the cells expressing the cell type-specific marker for hNSCs and nestin were identified (Fig. 4b_2). Furthermore, no significant change was found in the viability, proliferation, metabolic activity, and differentiation potential of NSCs after treatment with GQDs. Interestingly, the fluorescent C_{60} nanoparticles which could easily penetrate into cancer cells were not detected inside stem cells [135] and CdS QDs were shown to be cytotoxic to stem cells [136]. Therefore, such GQDs have a distinct advantage in terms of their penetrating power to stem cells. The surface charge and physicochemical nature of GQDs and C_{60} nanoparticles may play an important role for their ability to enter the stem cells, although no direct evidence has been reported yet. More in-depth research needs to be carried out to address this fundamental issue, which will help in the rational design of CDs for biomedical applications. Afterwards, green fluorescent 2,2′-(ethylenedioxy)bis(ethylamine)-carbon dots (EDA-CDs) prepared by Liu et al. were successfully used for labeling fixed mesenchymal stem cells (MSCs) [137]. The labeling of the fixed MSCs by the EDA-CDs was much more efficient, corresponding to much brighter fluorescence images and with the hyperchromatic nucleolus brighter than the other regions while for labeling live stem cells the cellular uptake is relatively less efficient. This combined with the observed more efficient internalization of the same CDs by the fixed stem cells may suggest selectivity of the live stem cells toward the dot surface functionalities.

Cancer stem cells (CSCs), as a subpopulation of stem-like cells within tumors, exhibit the characteristics of both stem cells and cancer cells [138]. They have the capacity to self-renew inside a tumor and to generate heterogeneous lineages of cancer cells that drive cancer progression, metastasis and drug resistance [139,140]. Therefore, they have been proposed as the cause of tumor relapse and are the relatively new target of cancer therapies. The labeling of CSCs poses a considerable challenge because of their particularity. Our group synthesized a turn-on orange-red fluorescent nanosensor based on rhodamine B derivative-functionalized graphene quantum dots (RBD-GQDs) for Fe^{3+} detection in pancreatic CSCs (Fig. 4c) [38]. Fe^{3+} binding to such GQDs (RBD-GQDs-Fe^{3+}) with strong orange-red fluorescence of 43% QY was first demonstrated to be a biomarker for pancreatic CSCs. From Fig. 4c, the morphology of pancreatic CSCs can be clearly discerned with the internalized RBD-GQDs-Fe^{3+}. Compared with other competing fluorescent nanomaterials, these GQDs are expected to be more practicable in biomedical applications due to the stability, the small size, the nontoxicity and the scope for straightforward surface functionalization.

Cell nucleus imaging

The cell nucleus is critical to various important cellular events, including metabolism, heredity and reproduction [141]. Nucleus-staining is the first step to revealing the nucleus morphology, to investigating the nuclear function, and to transferring the agent to the cell nucleus [142]. In most of cell imaging experiments, CDs were located only in the cytoplasm and cell membrane. Datta et al. for the first time reported the uptake of CDs into the cell nucleus [143]. CDs entered the nucleus due to their strong positive charge originating from the precursor with quaternary ammonium combined with their small sizes. Then Kang's group synthesized biomolecule-mimicking nitrogen-doped CDs (N-CDs) from dopamine by a neutralization heat strategy [144]. Cell imaging of the N-CDs validated their nucleus-staining efficiency with four kinds of cancer cells including rat pheochromocytoma cells (PC12),

human lung adenocarcinoma cancer cells (A549), human liver carcinoma cells (HepG2), and breast cancer cells (MD-MBA-231) as models. They indicated that the small size, surface positive charge and dopamine-mimicking groups of the N-CDs are critical to allow their entrance into the nucleus. In addition, the polyethylenimine functionalized GQDs (GQDs-PEI) acquired by Wang et al. were also rendered into the nucleus region [145]. They deduced that the nucleus permeability of GQDs-PEI may attribute to the ultra-small size and high concentration of positively charged nitrogen atoms of PEI.

Two-photon fluorescence imaging

Two-photon fluorescence imaging has the advantages of allowing a deeper penetration into living organisms, a lower tissue autofluorescence background and a less photodamage by avoiding harmful UV or blue excitations. The potential of CDs for two-photon luminescence microscopy with a femtosecond pulsed laser at 800 nm excitation was first demonstrated in MCF-7 cells [146]. The CDs exhibited bright fluorescence both on the cell membrane and in the cytoplasm. Before long, nitrogen-doped GQDs (N-GQDs) using dimethylformamide (DMF) as both solvent and nitrogen sources were synthesized by a facile solvothermal approach [6], and tested for two-photon imaging. The two-photon absorption cross-section (TPACS) of N-GQDs reached 48000 Göppert-Mayer units owing to the existence of a large π-conjugation and the strong electron denoting effect of the doped nitrogen atoms, which far surpassed that of the organic dyes and appeared comparable to that of the high performance semiconductor QDs. What is more, a deep penetration study in tissue phantom demonstrated that the N-GQDs can achieve a large imaging depth of 1800 μm, significantly extending the fundamental two-photon imaging depth limit. Recently, nitrogen-doped CDs (N-CDs) have also shown potential as two-photon fluorescence probes for high contrast bioimaging applications [147,148].

In vivo imaging

Because of the autofluorescence and light scattering background of biological specimens in short-wavelength region, fluorescent materials of choice for in vivo imaging are expected to emit in the long-wavelength region in order to provide a deeper light penetration into the specimens, resulting in a higher imaging contrast. Fluorescent CDs for in vivo imaging emitting in the red or NIR region are still challenging since most of the previously reported CDs emit only blue to green fluorescence. Wang's group first successfully used red fluorescent CDs with the emission peak at 640 nm for in vivo animal imaging by intravenous injection [149]. HeLa tumor-bearing nude mice were treated with intravenous injections of CDs. Fig. 5a_1 shows that the CDs accumulate in the tumor area through the enhanced permeability and retention (EPR) effect and significant fluorescence signal was observed in the tumor area in comparison with other tissues. The fluorescence intensity of CDs accumulated in the tumor areas quickly increased within 2–5 h post-injection, reached a plateau within 6–9 h post-injection, and steadily decreased over time. At 24 h post-injection, the mice was sacrificed, the excised tumor and liver tissue showed strong fluorescence intensity, whereas the spleen and heart showed very low signals (a_2) which is similar to the in vivo behavior of many other previously reported CDs.

Delivering imaging probes to brain tumors represents one of the most challenging in vivo tasks because of the blood-brain barrier (BBB) and the complex dependence on the probe size and surface properties. Recently Wang et al. developed polymer-coated nitrogen-doped CDs (pN-CDs) prepared by a facile direct solvothermal reaction for in vivo tumor targeting [150]. The pN-CDs having a diameter of 5–15 nm could expediently enter glioma cells and mediate glioma fluorescence imaging in vivo with good contrast via elevated passive targeting. Fig. 5b showed in- and ex-vivo imaging of glioma-bearing mice intravenously administrated with the pN-CDs at various time points post-injection. The highest fluorescent imaging was obtained at 30-min post-injection of the pN-CDs and enhanced accumulation of the pN-CDs was observed within the glioma based on the EPR effect. The accumulation of the prepared pN-CDs in this work within the glioma was much longer than some other reported CDs [151], suggesting their high potential for practical clinical application.

Cancer therapy applications of CDs

Cancer is one of the most deadly diseases facing humanity and current treatment methodologies are far from what is desired [152,153]. Photodynamic therapy (PDT), as one of the most effective treatments for cancer, has attracted tremendous research attention owing to its lower toxicity and higher selectivity compared to surgery, chemotherapy and radiotherapy [154,155]. PDT depends on the ability of photosensitizers (PSs) to transfer energy from lasers to tumour-dissolved oxygen to generate cytotoxic reactive oxygen species (ROS) that consequently induce irreversible damage of cancer cells. Markovic et al. and Christensen et al. firstly found that CDs could be used as PSs to generate ROS under the irradiation of blue light in vitro [154,155]. However, the blue light used in these studies can hardly penetrate through the tissue [156]. To unleash the full potential of ROS generation in vivo and the tumor treatment by CDs, the fluorescence of CDs should be tuned into at least the red or NIR region of the spectrum. Ge et al. prepared GQDs with a strong deep red emission by designing precursor molecules, polythiophene derivatives (PT2), as the carbon source (Fig. 6a) [24]. Through in vitro and in vivo studies, they demonstrated that GQDs could be used as PDT agents with unprecedented singlet oxygen ($^1O_2$) production via a multistate sensitization process, which provided a highly efficient cancer therapy. Immediately following these findings, they prepared CDs with a broad absorption band in the visible to NIR region (400–800 nm) and a red fluorescence emission peak at 640 nm using another conjugated polymer, polythiophene phenylpropionic acid (PPA), as the precursor (Fig. 6b) [149]. They first demonstrated that the red emissive CDs with a high photothermal conversion efficiency of 38.5% under 671 nm laser irradiation could act as thermal theranostics for cancer treatment in live mice, thereby significantly broadening the applications of CDs in photothermal therapy (PTT). CDs prepared by the research group using polythiophene benzoic acid as carbon source were shown to have dual photodynamic and photothermal effects under 635 nm laser irradiation with a $^1O_2$ generating efficiency of 27% and high photothermal conversion efficiency of 36.2%. The obtained CDs were used as a red-light-triggered theranostic agent for imaging-guided photodynamic-photothermal simultaneous therapy in vitro and in vivo within the therapeutic window (600–1000 nm) [157].

PDT depends on the ability of photosensitizers to transfer energy from lasers to tumour-dissolved oxygen (O_2) to generate cytotoxic $^1O_2$ for cancer treatment [158]. In most solid tumours, hypoxia is common because the oxygen supply is reduced by the impaired microcirculation and deteriorated diffusion [159]. Additionally, PDT may worsen the hypoxia further through oxygen consumption and vascular shutdown effects [160], thus the inadequate oxygen supply in tumour prevents PDT from achieving its full therapeutic potential [161–163]. Contrary to the generation of $^1O_2$ in PDT, photo-generation of anticancer nitric oxide (NO) radical is not limited by the supply of molecular oxygen, which may well complement the conventional PDT [164]. However, therapeutic applications of exogenous NO are usually limited by its short half-life and vulnerability to many biological substances [165–167], thus straightforward and precise control over NO delivery is critical to its therapeutic effects. To better control the NO release,

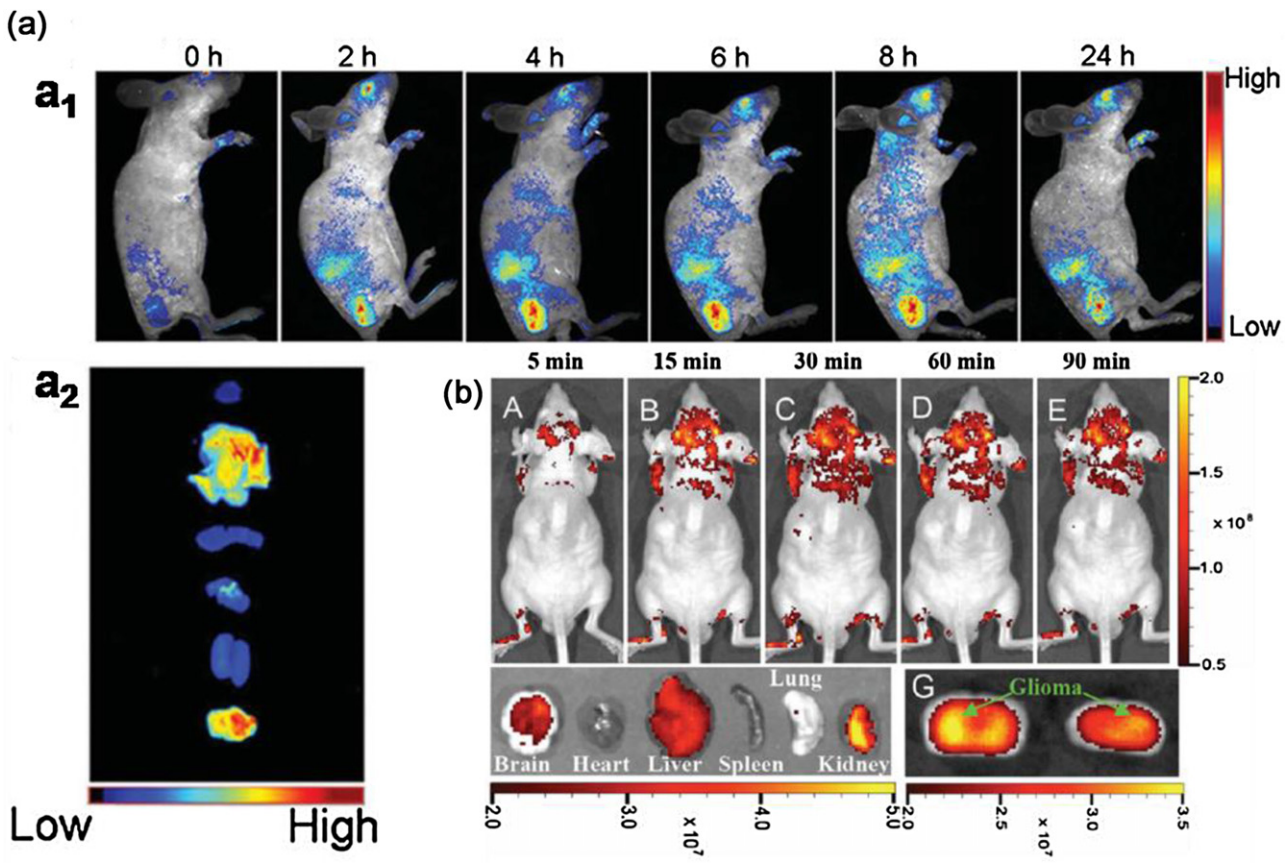

Fig. 5. (a_1) Real-time in vivo red fluorescence images after intravenous injection of CDs in nude mice at different time points. (a_2) Ex-vivo images of mice tissues (from top to bottom: heart, liver, spleen, lung, kidneys, tumor). Reprinted with permission from [149]. Copyright 2015 John Wiley and Sons. (b) In- and ex-vivo imaging of glioma-bearing mice intravenously administered with the pN-CDs. (A–E) Whole body imaging of the pN-CDs at various time points post-injection. (F) Ex-vivo imaging of major organs 90 min after pN-CDs administration. (G) Coronal imaging of the brain 90 min after pN-CDs administration. Black arrow represents the signal intensity (radiant efficiency) from weak (red) to strong (yellow). Reprinted with permission from [150]. Copyright 2015 John Wiley and Sons.

Xu et al. introduced a multifunctional NO-releasing nanosystem by covalently incorporating a photo-responsive NO-donor 4-nitro-3-(trifluoromethyl) aniline derivative and a mitochondrial targeting ligand triphenylphosphonium moieties onto CDs for mitochondrial-targeting, photo-controllable NO-releasing and cell imaging (Fig. 6c) [168]. Their study demonstrated that the combination of mitochondrial-targeting and highly controlled NO-releasing could cause a high toxic effect towards cancer cells by specifically damaging their mitochondria upon 400 nm light irradiation, providing new insights for exploiting NO in cancer therapy with the ultimate goal of maximizing the therapeutic action while minimizing side effects. Since the absorption window of NO photoprecursors used by Xu et al. [168] fell below the photo-therapeutic window (650–1350 nm) where light penetration through human tissue was restricted to only a few millimetres [169], two-photon excitation (TPE) which allowed excitation in the therapeutic window and permitted high spatial resolution in three dimensions were used in NO-photostimulated treatment modalities by Fowley et al. [170]. They reported a novel nanoconstruct in which carboxylic acid-terminated CDs were covalently linked to the NO photodonor nitroaniline derivative to give the nanohybrid (Fig. 6d). The photoinduced energy transfer occurs from the CDs core to the NO photodonor shell, generating the anticancer NO radical.

Another important therapeutic potential of CDs is their ability to serve as nanocarriers [171]. CDs are generally composed of a mixed phases of sp^2- and sp^3-hybridized carbon nanostructures in the form of conjugated carbon clusters functionalized with abundant periphery carboxylic groups, imparting them with suitability for subsequent functionalization with various organic, polymeric, inorganic or biological species by physisorption, π-π stacking, hydrophobic interaction, electrostatic attraction or chemical modifications [15,172]. These unique characteristics make CDs very suitable as delivery carriers for real-time monitoring the tracing of genes [77,173–177], anticancer drugs [178–185], and photosensitizers [186–190] in the cellular microenvironment. Liu et al. fabricated polyethylenimine (PEI)-functionalized CDs (CDs-PEI) by one-step microwave assisted pyrolysis of glycerol and branched PEI25k mixture (Fig. 7a) [77]. The elaborately fabricated CDs-PEI with excellent water solubility and bright multicolor fluorescence could mediate gene transfection in COS-7 and HepG2 cells with higher or comparable efficiency as well as lower cytotoxicity relative to pristine PEI25k. These results first suggested the potential of CDs for applications in gene delivery. Since then, several other reports have described the use of engineered CDs for gene delivery [173–177]. In 2013, Kim et al. reported a ternary complex between PEI-functionalized CDs, PEI-functionalized gold nanoparticles and plasmid DNA (pDNA) for in vitro transfection and real-time monitoring of plasmid cellular trafficking (Fig. 7b) [173]. Although PEI25k used in these studies is a highly effective gene transfection agent, the high charge density of PEI25k would limit the in vivo applications. Therefore, low molecular weight PEI modified with hydrophobic parts (i.e., Alkyl-PEI2k) which shows high gene transfection efficiency and good biocompatibility were used to synthesize composites of Alkyl-PEI2k and CDs (denoted as Alkyl-PEI2k-CDs) for in vivo delivery of siRNA and plasmid DNA (pDNA) by Wang et al. (Fig. 7c) [177]. They demonstrated gene expres-

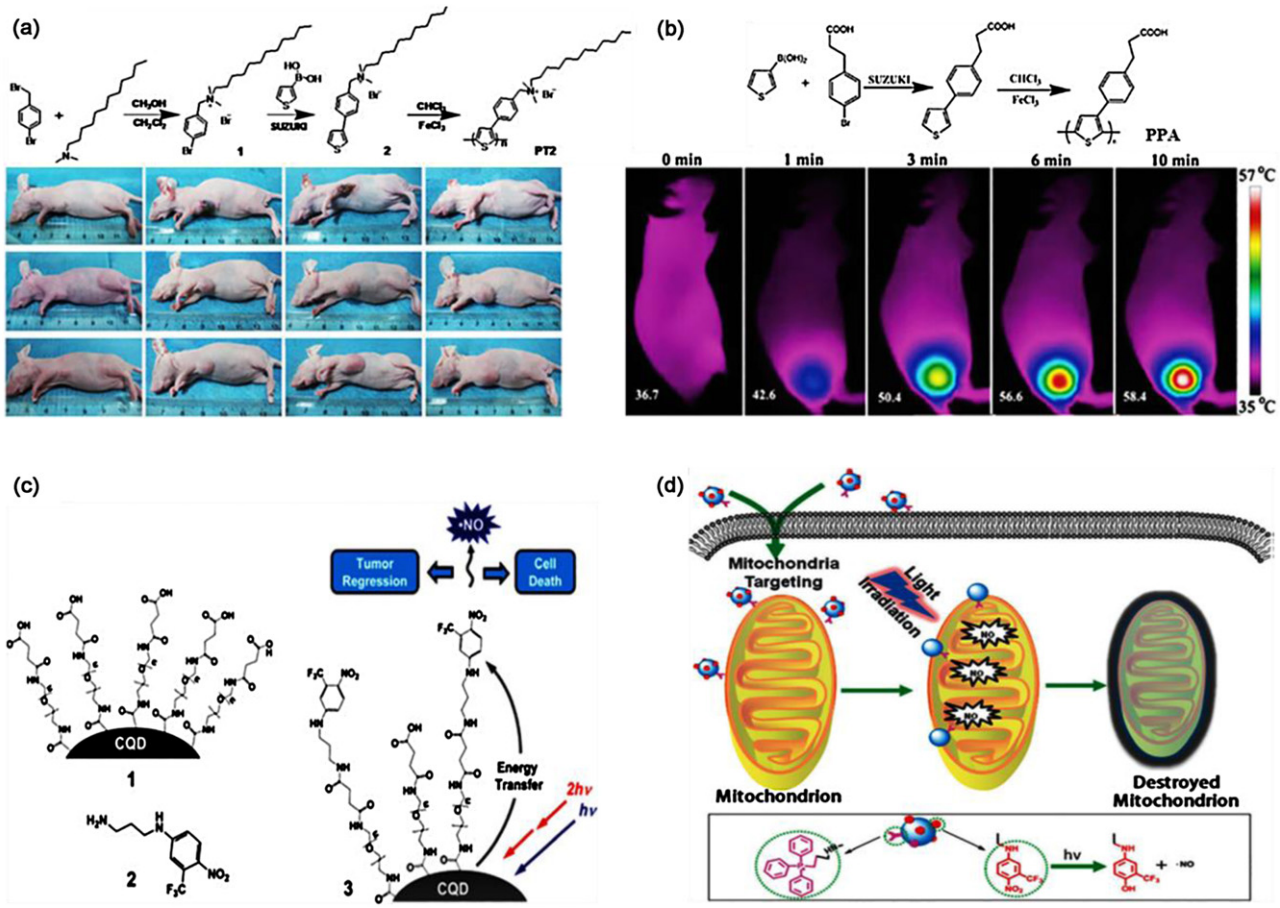

Fig. 6. The synthetic routes of PT2 (a) and PPA (b) used as carbon sources to prepare CDs for PDT or PTT, respectively. (a) Reprinted with permission from [24]. Copyright 2014 Nature Publishing Group. (b) Reprinted with permission from [149]. Copyright 2015 John Wiley and Sons. (c) The multifunctional NO-releasing nanosystem by covalently incorporating a photo-responsive NO-donor and a mitochondrial targeting ligand onto CDs for photo-controllable NO-releasing. Reprinted with permission from [168]. Copyright 2015 Royal Society of Chemistry. (d) Schematic illustration of the action of the CDs-based multifunctional system on the mitochondrion of a cancer cell. Reprinted with permission from [170]. Copyright 2015 Royal Society of Chemistry.

sion and silencing respectively after intratumoral administration of CDs-pDNA and CDs-siRNA complexes in a xenografted tumor mouse model, providing the first proof of the concept that CDs can mediate transfection in vivo.

Through chemical modifications, hydrophobic interactions or π-π stacking, multiple therapeutic molecules, including anticancer drugs doxorubicin (DOX), oxaliplatin (OXA) and epirubicin (EPI) as well as photosensitizers hypocrellin A (HA), chlorine e6 (Ce6), zinc phthalocyanine (ZnPc) and protoporphyrin IX, can be covalently bonded to CDs [191,192] or simply adsorbed onto the surfaces of CDs [172]. CDs can highly increase the water solubility of these hydrophobic drugs and facilitate their release in the often acidic conditions found within tumors [178,179,181,182,185]. Importantly, CDs or their assemblies can accumulate into tumors in vivo through either "passive" targeting by the enhanced EPR effect or "active" targeting by introduction of a targeting ligand for overexpressed receptors in tumor/vasculatures [172]. Tang et al. reported for the first time a direct and sensitive fluorescence resonance energy transfer (FRET)-based CDs drug delivery system (DDS) via a direct surface coupling strategy for the real-time monitoring of drug release [183]. As shown in Fig. 8a, CDs were first conjugated with amino-group terminated PEG (PEG-NH_2) and then covalently attached with folic acid (FA), an ideal ligand for folate receptors that were overexpressed in various types of human cancer [193]. Afterwards, DOX acted as an anticancer drug and an acceptor was adsorbed onto the surface of CDs used as a drug carrier and a donor via electrostatic interaction and π-π stacking to form a conjugate. The green fluorescence of CDs decreased and the red fluorescence of DOX increased when FRET occurred between CDs and DOX, while the FRET was weakened and the fluorescence of CDs recovered with the release of DOX from CDs surface. This change in FRET signal could be easily regulated by the release of DOX from the surface of CDs, thus allowing direct monitoring and quantification of the drug release process. Qiu et al. fabricated a multifunctional and biocompatible DDSs based on RGD (arginine-glycine-aspartic acid)-functionalized GQDs loading with DOX for the simultaneous tracking and targeted treatment of prostate cancer cells (Fig. 8b) [182]. Modification of the GQDs-based DDS with targeting (RGD) peptides facilitated the uptake of GQDs and consequentially enhanced the availability and effect of the carried DOX. Similarly, photosensitizer ZnPc were also loaded onto the surface of PEG-passivated CDs modified with FA (CDs-PEG-FA) for simultaneous biological imaging and targeted PDT by Choi et al. (Fig. 8c) [187]. The biocompatible and tumor-targeting CDs-PEG-FA selectively accumulated in tumors and activated ZnPc upon irradiation, which enhanced the selectivity and therapeutic efficacy of PDT both in vitro and in vivo. Drug carriers based on CDs possess distinct pharmacokinetic behavior compared to free molecules, which may not only enhance the tumor killing efficiency but also decrease toxicity in surrounding healthy tissue [178,186,188].

The ability of a single nano-object to perform multiple functions has made CDs vigorously encroaching biomedicine areas because practical applications often require disease detection, drug and photothermal treatments, and therapeutic efficacy monitoring,

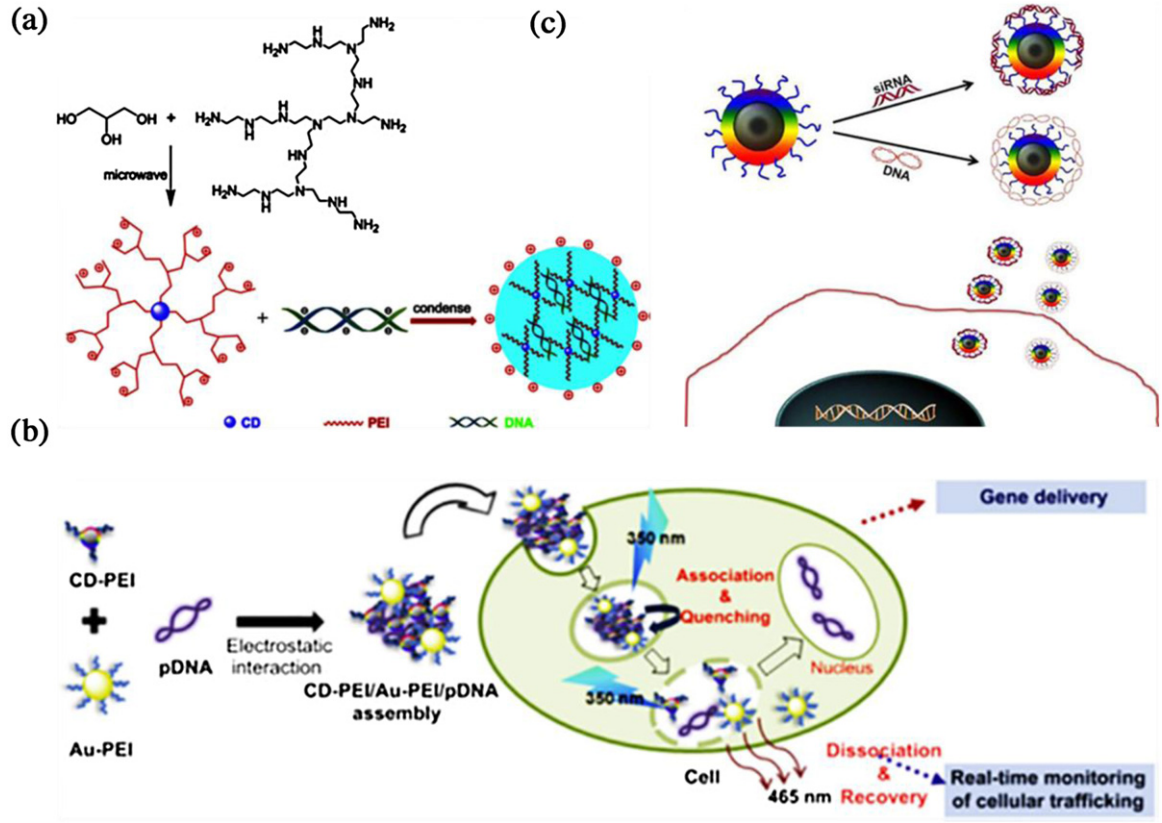

Fig. 7. (a) Depiction of the formation of CDs-PEI and CDs-PEI/pDNA complex. Reprinted with permission from [77]. Copyright 2012 Elsevier. (b) The gene delivery and real-time monitoring of cellular trafficking utilizing CDs-PEI/Au-PEI/pDNA molecular assembly of nanohybrids. Reprinted with permission from [173]. Copyright 2013 Elsevier. (c) The formation of Alkyl-PEI2k-CDs/siRNA complex and delivery into cancer cell. Reprinted with permission from [177]. Copyright 2014 John Wiley and Sons.

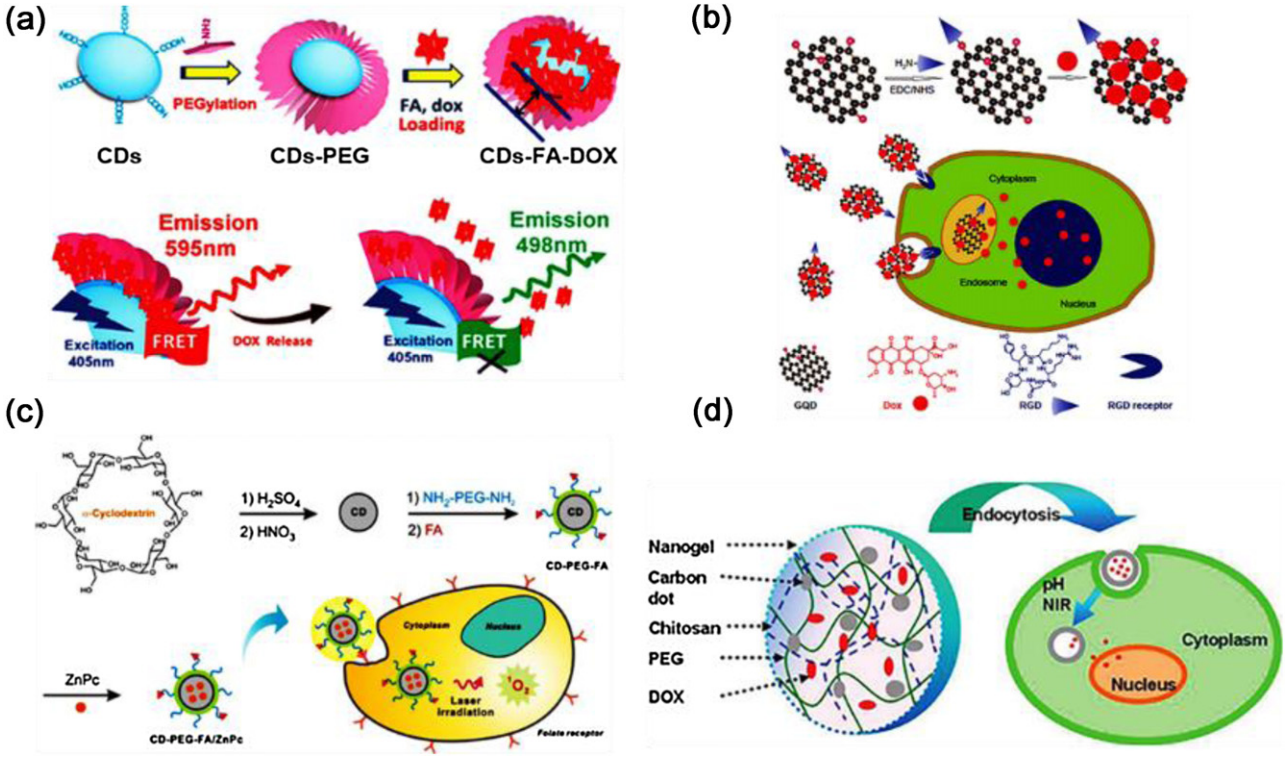

Fig. 8. (a) A schematic representation of the surface coupling chemistry for FRET-CDs-DDS for drug delivery. Reprinted with permission from [183]. Copyright 2013 John Wiley and Sons. (b) The multifunctional GQDs for the traceable, targeted delivery of DOX and their interactions with cancer cells. Reprinted with permission from [182]. Copyright 2015 Dove Medical Press. (c) The preparation of CDs from α-cyclodextrin and targeted PDT with FA functionalized CDs loaded with ZnPc (CDs-PEG-FA/ZnPc). Reprinted with permission from [187]. Copyright 2014 John Wiley and Sons. (d) PEG-chitosan@CDs hybrid nanogels for pH/NIR dual-responsive drug release and two-photon fluorescence cellular imaging. Reprinted with permission from [198]. Copyright 2015 John Wiley and Sons.

simultaneously [194–196]. A class of multifunctional core-shell hybrid, which integrated fluorescent CDs, magnetic Fe_3O_4 nanocrystals, Au nanocrystals, thermo-responsive poly(NIPAM-AAm)-based hydrogel, nonlinear PEG, chitosan and anticancer drug into the porous carbon shells, were designed for optical temperature sensing, magnetic/NIR-thermally responsive drug delivery, multicolor cell imaging and enhanced effect of PTT, respectively [185,197–199]. For example, Wang et al. designed PEG-chitosan@CDs hybrid nanogels by integrating nonlinear PEG, chitosan, and graphitic CDs into a single nanoparticle for simultaneous two-photon fluorescence (TPF) bioimaging, pH and NIR light dual-responsive drug release, and synergistic therapy (Fig. 8d) [198]. The hybrid nanogels could enter the intracellular region and lighted up tumor cells under the excitations of both UV and NIR lasers, and the pH-sensitive volume phase transition of the hybrid nanogels could facilitate an on-site pH-regulated drug release and modulate the surface properties of the embedded CDs to sense the environmental pH change over the physiologically important range of 5.0–7.4. Furthermore, the thermoresponsive properties of the hybrid nanogels could also trigger the drug release under the irradiation of NIR light through the photothermal conversion ability of the embedded CDs. Such a multifunctional intelligent hybrid nanogels enabled a combined chemo-photothermal treatment to provide a high therapeutic efficacy.

Optoelectronic applications of CDs

Benefiting from the high specific surface areas, unique optoelectronic properties such as high electron mobility, long hot-electron lifetimes, ultrafast electron extraction, tunable bandgaps and strong stable fluorescence, the emerging quantum-sized CDs should hold great promise for efficient optoelectronic applications. In the following, we will roundup the most rcent CDs-related researches focused on LEDs, solar cells and solar fuels.

Light-emitting diodes

Light-emitting diodes (LEDs) have been the subject of intense academic research for years, aiming at their potential applications in liquid-crystal displays and full-color displays and as the next generation of lighting sources in our daily life [200,201]. As a new kind of fluorescent QDs system, the emerging quantum-sized CDs appear to be a promising alternative to rare earth-based expensive phosphors and toxic metal-based semiconductor QDs in LEDs due to their tunable stable fluorescence emission, low cost and low environmental impact. The large PL bandwidth of CDs make them good candidates for fabricating white LEDs (WLEDs), which have become an important energy-saving technology for the sustainable development of our society due to their projected long working life time, low power consumption, fast response time and compact size. Therefore, some efforts have been made to realize the great potential applications of CDs in LEDs.

Generally, the applications of CDs in LEDs can be divided into two types based on the excitation mode: One is based on the optical excitation, which results in color-conversion LEDs using CDs as the phosphors component, and the other is through direct electrical excitation, resulting in LEDs based on the electroluminescence (EL) of CDs.

LEDs based on the PL of CDs

The LEDs based on the PL of CDs usually consist of UV or blue chips and fluorescent CDs. The CDs are used as phosphors and can be excited by the strong UV or blue light from EL of the chips. One of the problems with the powders of CDs is the very weak fluorescence due to aggregation induced quenching (AIQ) effect, which greatly hampered the development and applications of CDs in LEDs. To avoid the AIQ effect, many groups have demonstrated that CDs embedded in solid matrices such as borax (as is illustrated in Fig. 9a) [52], silicone [202–204], starch [205], cellulose nanofiber [206], and resin [207–211] can preserve the fluorescence, renewing the promise of CDs in WLEDs. Tang et al. showed GQDs as an excellent light converter by coating a layer of their GQDs onto a commercially available blue LEDs centered at 410 nm for the first time [74]. Upon the coating of the GQDs, the intensity of the blue light weakened and a broad band peaking at about 510 nm arose. Concomitantly, the Commission International d'Eclairage (CIE) chromaticity coordinates of the LEDs shifted from (0.242, 0.156) to (0.282, 0.373), demonstrating the ability of GQDs to convert blue light into white light. The behavior of color conversion was understood as the mixing of the 410 nm emission from the blue LEDs and a broad emission at 510 nm given by GQDs under the 410 nm excitation. Moreover, Chen et al. fabricated WLEDs with UV chips and fluorescent CDs with PL QY up to 47% as phosphors prepared by unzipping photonic crystals, and realized warm white light with color coordinates of (0.45, 0.44) for the first time as shown in Fig. 9b [212]. Before long, they synthesized CDs through a one-step pyrolysis from N-acetylcysteine with broad yellow emission spectrum and WLEDs with CIE coordinates realized at (0.34, 0.35) close to the pure white light emission were fabricated by combining the yellow emitted CDs with blue GaN-based LED chips [213]. Rhee et al. fabricated large-scale (20×20 cm) freestanding luminescent films of the CDs based on a poly(methyl methacrylate) matrix, which not only provide mechanical support but also disperse the CDs to prevent solid-state quenching [214]. Finally, they demonstrated WLEDs consisting of the films as color-converting phosphors and InGaN blue LEDs as illuminators, and the WLEDs exhibited no temporal degradation in the emission spectrum under practical operation conditions (Fig. 9c). Although a single phosphor can be easily combined with blue LEDs for WLEDs, the resulting correlated color temperature (CCT) can not be readily varied without compromising the high color rendering index (CRI). Coating UV LEDs with multicolor phosphors can maintain high CRI by changing the ratio of the phosphors. Therefore, in order to enhance the CRI and tune the CCT of WLEDs, Sun et al. fabricated WLEDs which integrated high PL QY blue CDs with yellow and red Cd-free zinc copper indium sulfide (ZCIS) core/shell QDs, which is shown in Fig. 9d [215]. The as-prepared WLEDs exhibited a very high CRI of 93, exceeding that of the YAG:Ce based commercial WLEDs (CRI < 75). Thereafter, Sun et al. further realized WLEDs with high CRI (85–96) and widely variable CCT (2805–7786 K) by combining three phosphors based on blue CDs, green and red polymer dots (Fig. 9e). The WLEDs showed excellent color stability against the increasing current because of the similar response of the tricolor phosphors to the UV light variation [216].

Though LEDs based on the PL of CDs have been demonstrated by incorporating CDs into solid matrices, the introduction of a thick solid matrix layer will depress the luminescence from chips and also increase the costs. The best way is to achieve high-quality luminescence in the solid state for fluorescent CDs and then directly use these materials as phosphors in LEDs. Li et al. prepared intercrossed carbon nanorings (CNRs) with very pure hydroxyl surface states for the first time, which enabled them to overcome the AIQ effect, and to emit yellow-orange luminescence in both colloidal and solid states (Fig. 10a). As a direct benefit of such scarce solid luminescence from CNRs, they were used as low-cost and environment-friendly phosphors on blue chips, and hence WLEDs were achieved with optimized color coordinate of (0.28, 0.27), which is close to pure white light (0.33, 0.33) [25]. Through surface modification of CDs or interparticle spacing control their aggregates, tunable solid-state fluorescence (SSF) of nitrogen-doped CDs (NCDs) has been successfully obtained for the first time. WLEDs was further realized by taking advantage of the otherwise undesirable

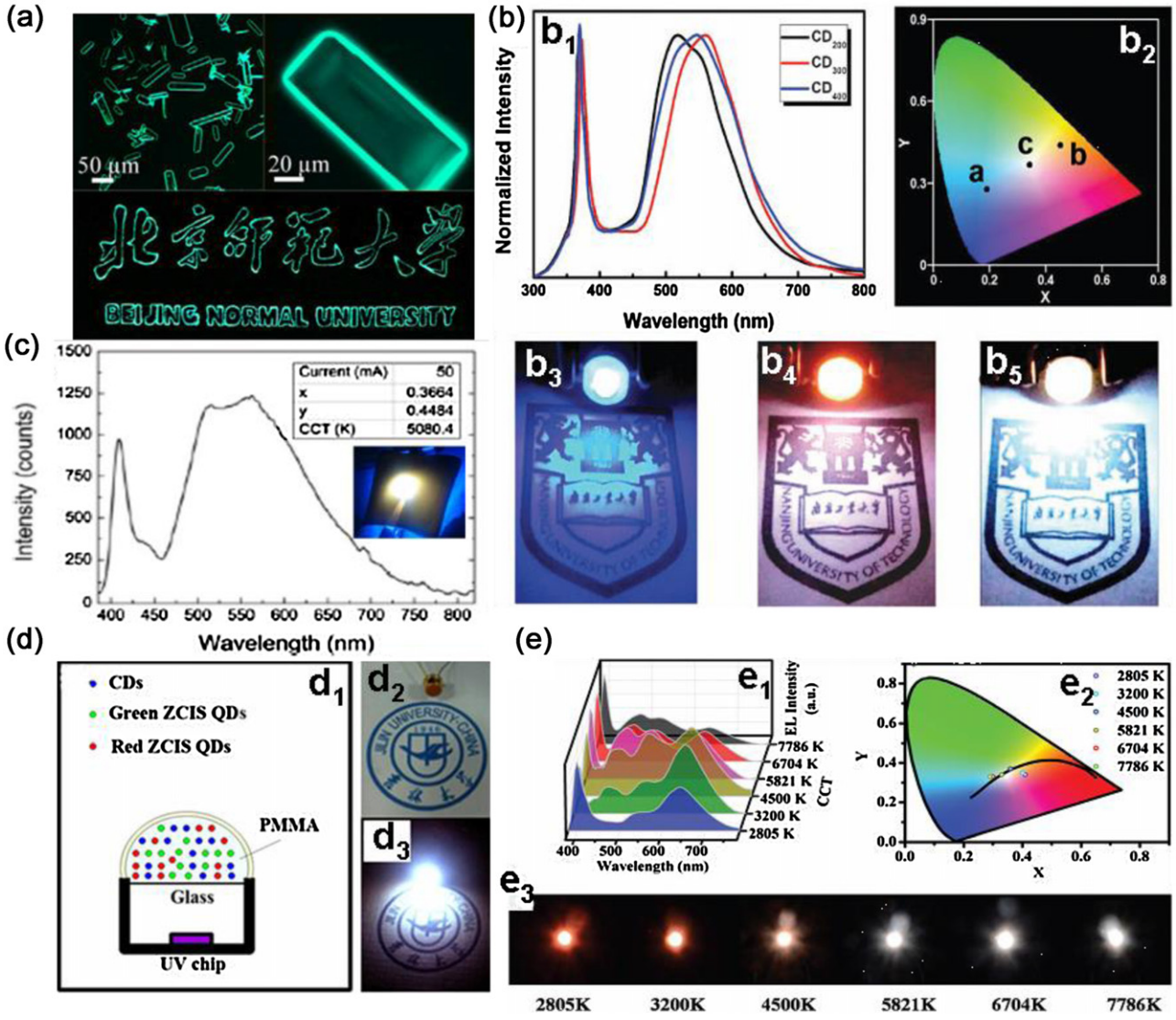

Fig. 9. (a) Fluorescence microscopy images and graphic patterns on a copper piece of B-GQDs crystals obtained by evaporating B-GQDs borax aqueous solution at room temperature. Reprinted with permission from [52]. Copyright 2014 Elsevier. (b) Emission spectra, CIE 1931 chromaticity coordinates and photographs of the corresponding LEDs. Reprinted with permission from [212]. Copyright 2012 Royal Society of Chemistry. (c) Emission spectra, CIE chromaticity coordinate and photograph of the WLEDs. Reprinted with permission from [214]. Copyright 2013 American Chemical Society. (d) Schematic diagram and the photographs of the WLEDs without and with biased current. Reprinted with permission from [215]. Copyright 2014 AIP Publishing. (e) EL spectra, CIE color coordinates and true-color images of various WLEDs. Reprinted with permission from [216]. Copyright 2015 Royal Society of Chemistry.

aggregation, which greatly simplified the preparation process of LEDs and other optoelectronic devices and hence reduced the cost compared with existing methods (Fig. 10b) [217]. Except the wide applications of CDs as phosphors for fabrication WLEDs, Rhee et al. fabricated LEDs exploiting CDs surface functionalized with para-substituted anilines as a phosphor, converting UV light to a variety of colors (Fig. 10c) with the aid of their excellent fluorescent QY and long-term stability [218].

However, up to now, the research of the CDs-based LEDs is still at an early stage with relatively low efficiencies compared with well developed QDs-LEDs. Luminous efficiency and CRI are important parameters to evaluate the quality of WLEDs, and it is still difficult to obtain CDs-based WLEDs with high CRI and high luminous efficiency due to the low QY of the long wavelength emission from CDs. Therefore, new strategies for large-scale production of CDs with high QY of the long wavelength emission beyond the blue light region need to be developed for the LED application.

LEDs based on the EL of CDs

For applications in EL devices, CDs can also be used as an active emission layer sandwiched in a multilayer device structure. The first electrically driven LEDs based on CDs was reported by Gupta et al. with the fabrication of organic LEDs (OLEDs) based on GQDs [119]. Mixtures of methylene blue functionalized GQDs (MB-GQDs) doped in poly(2-methoxy-5-(2-ethylhexyloxy)-1,4-phenylenevinylene) (MEH-PPV) with different GQDs doping concentrations were employed as the active emission layer and tested in OLEDs under the optimized conditions. As shown in Fig. 11a, the turn-on voltage of the device decreased from about 6 V for the pure MEHPPV sample to about 4 V for MEH-PPV with 1% MB-GQDs. At a higher concentration of 3% MB-GQDs, charge trapping as well as a shortening effect occurred, possibly due to agglomeration. The maximum light-emission intensity increased with the addition of MB-GQDs to MEH-PPV, directly reflecting the enhanced internal quantum efficiency. In mechanism, the MB-GQDs dispersed in the MEH-PPV afforded additional

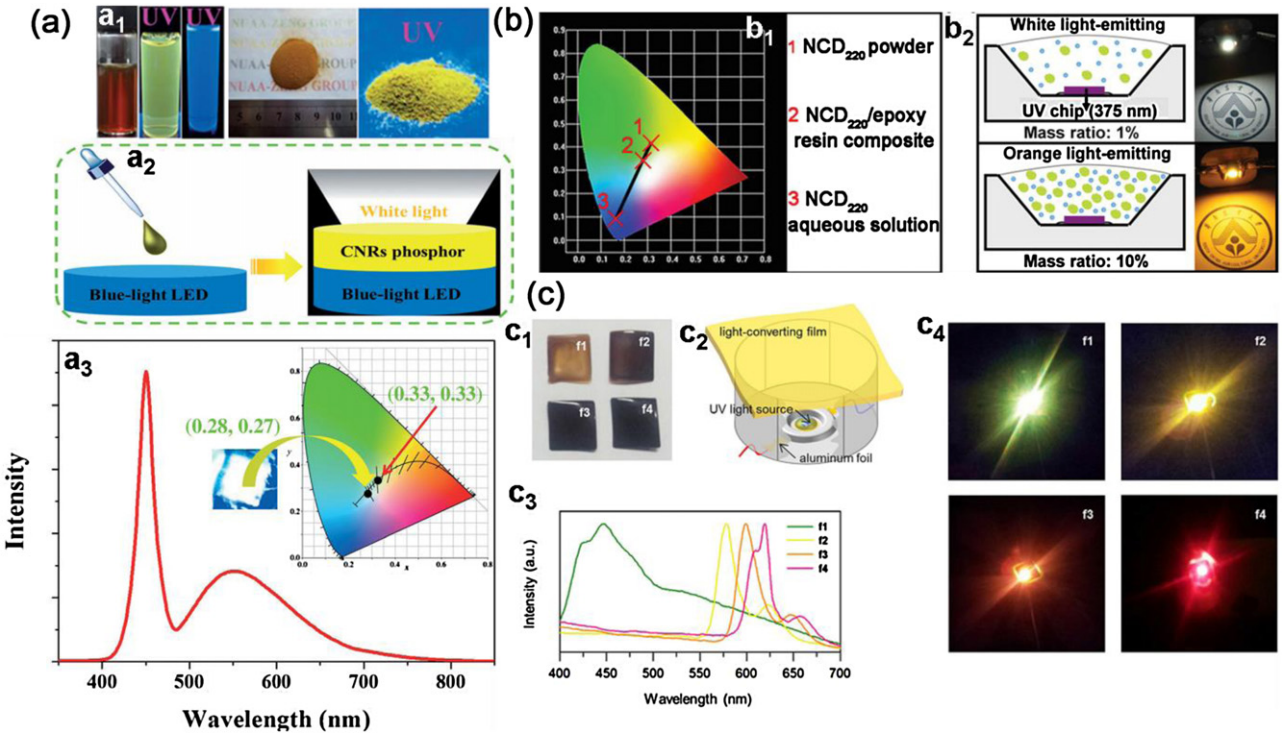

Fig. 10. (a_1) Images of CNRs dispersions and powders under sunlight and UV light, (a_2) Fabrication strategy of WLEDs based on blue LEDs, (a_3) EL spectra of WLEDs. The insets are the digital image of the device and the corresponding CIE chromaticity diagram. Reprinted with permission from [25]. Copyright 2015 John Wiley and Sons. (b_1) CIE coordinates of NCD_{220} powder, composite, and NCD_{220} aqueous solution under UV light, (b_2) Schematic and photographs of the white and orange LEDs. Reprinted with permission from [217]. Copyright 2016 John Wiley and Sons. (c_1) Photographs of light-converting films, (c_2) Construction of LEDs, (c_3) Emission spectra and (c_4) photographs of LEDs. Reprinted with permission from [218]. Copyright 2015 Nature Publishing Group.

electrical transport paths that improved charge injection and consequently the carrier density, therefore resulting in a lower turn-on voltage. After that, WLEDs based on an emissive layer of CDs passivated with 1-hexadecylamine which was sandwiched between a poly(ethylenedioxythiophene):polystyrenesulphonate (PEDOT:PSS) hole injection layer and a 1,3,5-tris(*N*-phenylbenzimidazol-2-yl) benzene (TPBI) electron transport layer have been successfully demonstrated for the first time by Wang et al. [219]. A maximum external quantum efficiency of 0.083% at a current density of 5 mA cm^{-2} with a CRI of 82 and CIE coordinates of (0.40, 0.43) is realized, indicating that CDs have great potential to be an alternative phosphor for fabricating white light EL devices.

Some great progress has been made recently for CDs in the EL device applications. Rhee et al. reported the synthesis of a range of the GQDs with certain size distributions via amidative cutting of tattered graphite [101]. The energy gaps in such GQDs are narrowed down with increasing the size, showing colorful PL from blue to brown. Finally, they demonstrated OLEDs employing 4,4′-bis(carbazol-9-yl)biphenyl (CBP) layer as a host and a series of the GQDs as a dopant (Fig. 11b). In their system, electrons and holes are injected by an electrical bias into CBP through TPBI and GraHIL, respectively, and then transferred from CBP to the GQDs, of which the energy levels are placed inside those of CBP. The largest external quantum efficiency (EQE) of the devices was ca. 0.1%, which is the first meaningful report on the EL of GQDs. However, such performance is quite inferior to that of the state-of-the-art OLEDs and QDs based LEDs, presumably due to the relatively low QY (about 10%), decreased contact area with host molecules, too much deep HOMO levels, and bulky ligand molecules hampering efficient energy transfer and direct charge injection to the GQDs. Interestingly, Zhang et al. fabricated LEDs with driving current controlled color change from blue to white based on highly blue fluorescent CDs as active emission layer as illustrated in Fig. 11c [220]. The devices consist of a CDs emissive layer sandwiched between an organic hole transport layer and an organic or inorganic electron transport layer fabricated by a solution-based process. By tuning the device structure and the injecting current density, they can obtain multicolor emission of blue, cyan, magenta, and white from the same CDs. This color variability phenomenon was originated from the presence of three recombination mechanisms in a single CDs emitting layer. Therefore, one can envisage creating a multicolor single pixel driven by the current density or voltage. This interesting current density-dependent emission is useful for the development of colorful LEDs. More recently, Kim et al. fabricated white polymer LEDs (PLEDs) using graphene oxide quantum dots (GOQDs) prepared by a modified hydrothermal deoxidization method blended poly(N-vinyl carbazole) (PVK) as emissive layer [221]. Simple device structure was used to reveal the origin of EL by excluding the contribution of and contamination from other layers. The brightness of the white EL emission was just about 1 cd/m^2 due to the relative low QY of GOQDs as shown in Fig. 11d_1. The energy transfer and interaction between the PVK host and GOQDs guest were investigated using steady-state PL, time-correlated single photon counting (TCSPC) and DFT calculations, and revealed that white EL emission from the PLEDs originated from the hybridized GOQDs-PVK complex emission with the contributions from the individual GOQDs and PVK emissions (Fig. 11d_2). As observed in the energy diagram in Fig. 11d_3, the energy levels of GOQDs are located within those of the PVK, and have a small energy barrier for charge injection from both electrodes; therefore, direct charge injection is possible in this system. Thus, the EL emission of GOQDs could have originated from both energy transfer from PVK host and direct charge injection to GOQDs.

Compared with the high performance LEDs fabricated by using the well developed Cd^{2+}-based semiconductor QDs or recently dis-

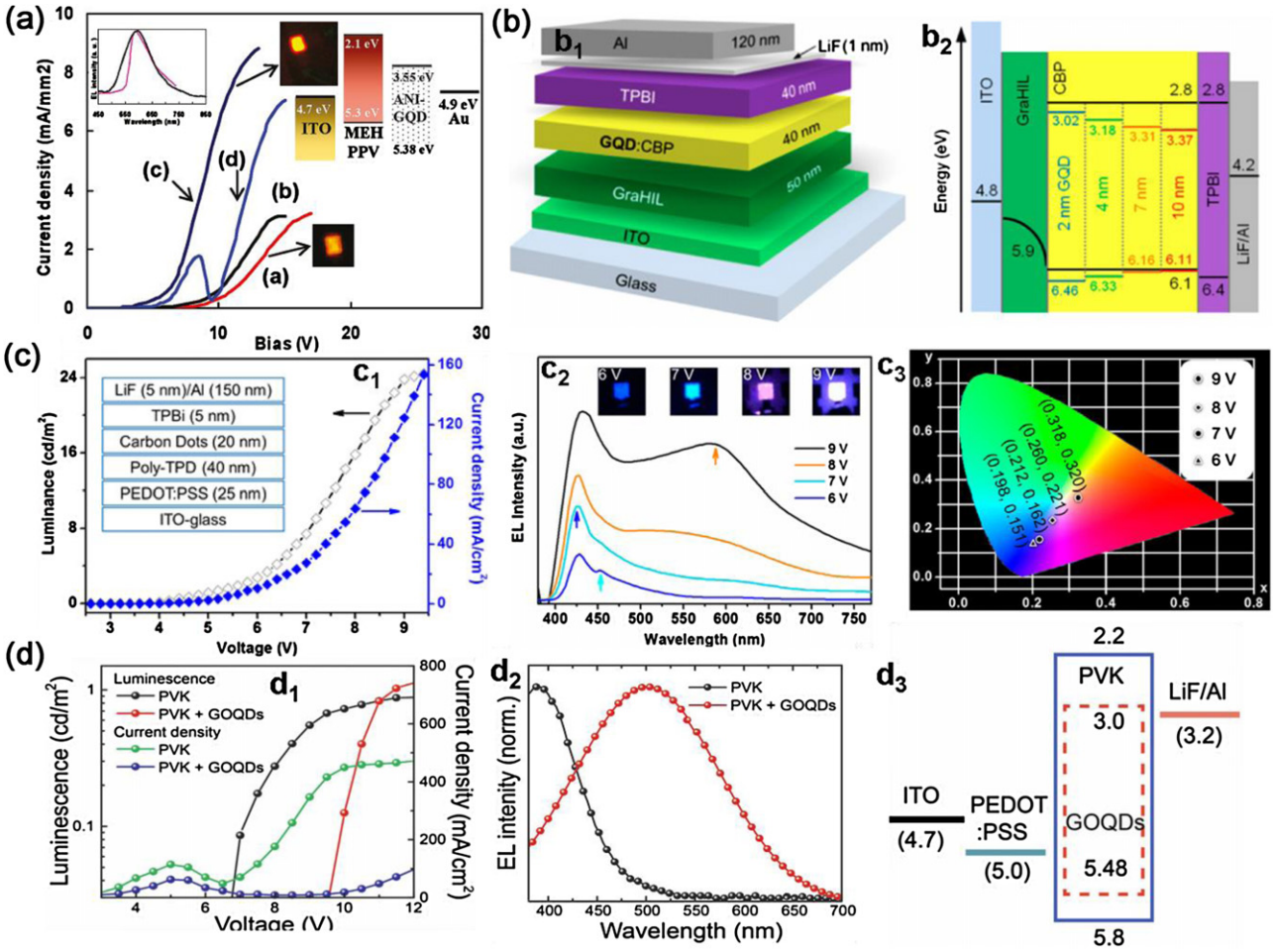

Fig. 11. (a) Current density of MEH-PPV with different concentrations of MB-GQDs as a function of the applied voltage. Reprinted with permission from [119]. Copyright 2011 American Chemical Society. (b) Physical and electronic structures of OLEDs employing the GQDs. Reprinted with permission from [101]. Copyright 2014 American Chemical Society. (c_1) Current density and brightness of the CDs-LEDs, (c_2) EL spectra and true color photographs of blue, cyan, magenta, and white emissions, (c_3) CIE coordinates of the CDs-LEDs operated under different voltages. Reprinted with permission from [220]. Copyright 2013 American Chemical Society. (d_1) Current density and brightness of PLEDs using pristine PVK and GOQDs blended PVK as emissive layers, (d_2) EL spectra and schematic energy diagram (d_3) of PLEDs. Reprinted with permission from [221]. Copyright 2015 Nature Publishing Group.

covered inorganic halide perovskite QDs which possess extremely high QY (70–95%) and narrow full width at half maximum (FWHM < 35 nm) as active emission layer [222–224], the efficiencies of the CDs-based EL LEDs are still relatively low. However, the research of CDs-based EL LEDs is still at a very early stage, and more in-depth studies are warranted due to the tunable stable fluorescence emission, low cost and low environmental impact of CDs. There are two key challenges facing the EL of CDs: material developments by synthesizing CDs with much higher QY in the solid state and thin films, as well as the carrier (holes and electrons) transport property of CDs with a conjugated surface and optimization of the charge injection with better controlled device fabrication through energy level matching by adding and tuning the thickness of hole transport layer or electron transport layer.

Solar energy conversion

CDs usually possess a wide range of light absorption tailing into the visible region, which is beneficial for their applications in solar energy conversion including solar cells (SCs) and solar fuels. In fact, CDs were utilized as a sensitizer in a dye-sensitized solar cell [225], but the low power conversion efficiency (PCE) (0.13%) due to the low short-circuit current density resulting from the severe surface recombination of photoinduced charges limited the further application of CDs as a hot carrier chromophore [226]. In organic solar cells, GQDs have been widely used as electron acceptors analogous to fullerenes with respect to the active layer of poly(3-hexylthiophene) (P3HT) [53,119]. Though the efficiency of this device is still low (~1%), it is expected that GQDs or CDs are promising alternatives to the expensive fullerenes as electron acceptors. The CDs also served as an electron blocking layer in the CDs/silicon nanowire arrays core-shell heterojunction solar cells [227,228]. Impressively, an optimum power conversion efficiency of 9.10% was obtained by tuning the CDs layer thickness. Up to now, CDs have been used in many kinds of SCs, such as dye (dot)-sensitized SCs [229], organic SCs [230,231] and silicon based SCs. Recently, we inserted a sub-monolayer layer of GQDs between the perovskite and the mesoporous titanium dioxide layers in a typical perovskite solar cell (Fig. 12a_1) [26]. The results of photocurrent-voltage curve, photocurrent quantum efficiency and transient absorption measurements showed that the GQDs could serve as a superfast bridge to facilitate the electron injection from the halide perovskite into the titanium dioxide, leading to a significantly enhanced photocurrent and PCE of the corresponding solar cells (from 8.81% to 10.15%, see Fig. 12a_2). This work indicated the possibility of collecting hot electrons from the photoexcited perovskite due to the rather slow cooling of the hot electrons. Further work on GQDs accelerated electron injection may allow the opti-

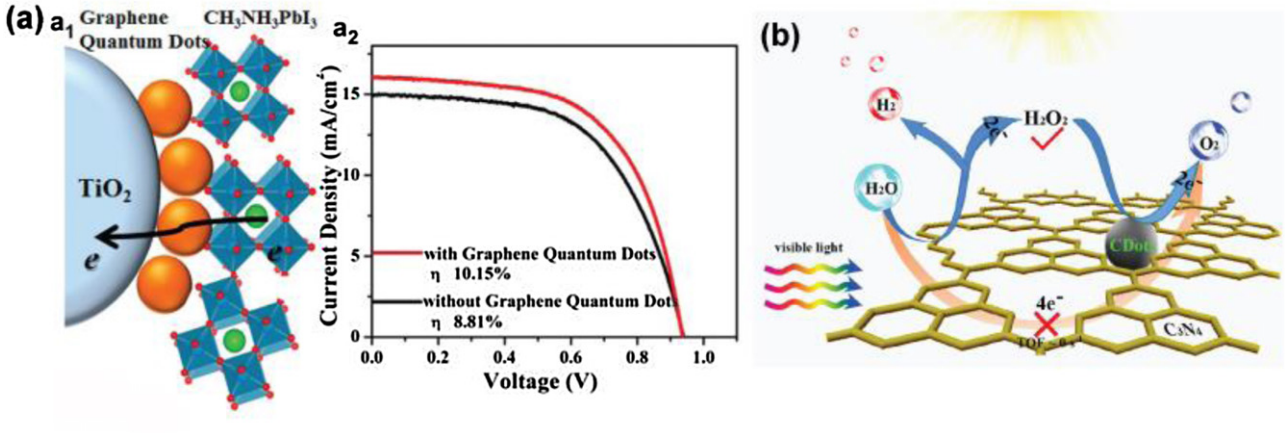

Fig. 12. (a_1) Schematic representation of the perovskite solar cell device structure, (a_2) Current density-voltage curves for the best-performing solar cells. Reprinted with permission from [26]. Copyright 2014 American Chemical Society. (b) The proposed reaction mechanism for visible-light-driven water splitting by CDs-C_3N_4. Reprinted with permission from [17]. Copyright 2015 The American Association for the Advancement of Science.

mization of hot carrier extraction before cooling down to the band edges, opening up new pathways for future developments of new generation solar cells.

CDs have also been popular in the pursuit of other solar energy conversion pathways, especially as photocatalysts in the water-splitting for hydrogen and the reduction of carbon dioxide (CO_2) into small organic molecules.

Again with the absorption of CDs overlapping with the solar spectrum for much of the visible light region, CDs have been explored as photocatalysts for H_2 generation from water-splitting. Cao et al. used PEG-functionalized CDs coated with gold or platinum metal for the visible-light photocatalytic H_2 generation from water [232]. The observed highest hydrogen production rate was about 9.1 μmol/h, which is higher than the rate obtained with neat TiO_2 photocatalysts. More popular and effective have been the photocatalysts based on CDs nanocomposites, in which the CDs essentially serve the role of visible-light photosensitizer. Understandably, due to the large rigid sp^2 π-conjugated structure, CDs exhibit excellent electron transfer/reservoir properties and can function as a good photocatalyst as the photoinduced electron-hole pairs can be efficiently separated. Nanocomposites of CDs have been developed with various nanostructures such as TiO_2 [233–235], ZnS nanospheres [236], CdSe [237], Ag [238], TaON [239], Ni complex [240], Cu_2S nanowire arrays [241] and $BiVO_4$ inverse opal [242]. The nanohybridization has remarkably enhanced the photocatalytic and photoelectric properties of CDs.

CDs not only serve the function of dyes in dye-sensitized semiconductor photocatalysts but also can participate directly in splitting water [243]. Visible light (>420 nm) irradiation on nitrogen-doped graphene oxide-quantum dots (NGO-QDs), which exhibited both p- and n-type conductivities, resulted in simultaneous H_2 and O_2 evolution from pure water at an H_2:O_2 molar ratio of 2:1. This work demonstrated the potential to design metal-free, cost-effective, and environmentally-friendly photocatalysts for overall water-splitting under solar illumination. CDs also possess high catalytic activity for H_2O_2 decomposition. By heating a mixture of ammonia-treated CDs and urea powder, a metal-free efficient photocatalyst CDs-C_3N_4 composites was fabricated and exhibited excellent water splitting performance under visible light irradiation (Fig. 12b) [17]. In contrast to the conventional one-step four-electron reaction, CDs-C_3N_4 photocatalyzed the water splitting into hydrogen and oxygen via the stepwise two-electron/two-electron pathway. Here C_3N_4 is responsible for the first step (photocatalysis), and CDs are responsible for the second step (chemical catalysis). The composite nature of the catalyst provides sufficient proximity between the H_2O_2 generation sites on the C_3N_4 surface and the CDs so that H_2O_2 decomposition and O_2 generation in the second stage can be efficient. CDs also increase the light absorbance and thus the quantum efficiency of water splitting. The highest quantum efficiency of 16% was obtained and the overall solar energy conversion efficiency reached up to 2.0%. Moreover, the CDs-C_3N_4 maintained long-term stability for at least 200 days, and the catalyst was dried and reused 200 times with a high rate of hydrogen and oxygen production. These results showed the promise of CDs-C_3N_4 as a highly efficient and stable photocatalyst for visible light-driven water splitting.

Photocatalytic conversion of CO_2 into small molecular fuels is considered as not only an alternative to photovoltaics in the harvesting of solar energy but also a solution of carbon sequestration. It has been demonstrated that CDs with surface passivation by amino or other molecules are capable of serving as visible-light photocatalysts for CO_2 reduction in aqueous solution [232]. There is obviously plenty of room for further improvement in the development of these CDs-based photocatalysts for CO_2 conversion.

Conclusions and perspectives

In this review, we have surveyed the latest exciting researches about the synthesis, structure and optical properties of CDs with a short critical survey and then address in great detail their advanced applications in biomedicine and optoelectronics. Mainly discussed are their applications in bioimaging with emphasis on stem cells imaging including normal and cancer stem cells, cell nucleus imaging, two-photon fluorescence imaging, red or NIR emission for in vivo imaging, cancer therapy including PDT, PTT and chemotherapy, and optoelectronic applications including LEDs and solar energy conversion. There is no doubt that the development of CDs for biomedical and optoelectronic applications has seen a great progress within a short time. However, the research is still at its early stage in terms of fundamental understanding and practical applications.

First of all, there are still many issues to be settled for further development. One of the most controversial fundamental issues of CDs is the PL mechanism. Further experimental verification and theoretical calculations are badly desired to provide a coherent picture. Moreover, CDs with a high QY comparable to traditional semiconductor QDs at longer wavelengths beyond the blue light region are yet to be synthesized on a large-scale through facile methods.

For bioimaging, although low toxicity of CDs has been established both in vitro and in vivo, long-term toxicity and precise toxicological effect of CDs need to be evaluated, which is utterly important for their biomedical application, especially in clinical use. CDs with bright fluorescence emissions falling in the NIR (750–900 nm) and NIR-II (1000–1700 nm) spectral regions or upconversion luminescence within the biological window are more appropriate for bioimaging. Especially, CDs fluorescing in the long NIR-II region (1000–1700 nm) can afford even deeper penetration than in the traditional NIR region (750–900 nm), and thus are highly desired. More elaborate designs and synthesis of CDs that allow to label stem cells, even the nucleus of stem cells, are urgently needed due to the important role of stem cells in cancer progression, metastasis and drug resistance. Moreover, the exact mechanism with which CDs interact with stem cells has not been understood at this stage and should be further addressed in the near future, which would guide the design of CDs for specific biomedical use. In addition, the potentiality of CDs-based nanoprobes as a platform for dual- or multi-modality bioimaging agents including magnetic resonance imaging or photoacoustic imaging need to be further explored. New cancer therapies that combine CDs, which can label stem cells even the nucleus of stem cells, with therapeutic agents such as PDT, PTT agents or anticancer agents are expected to receive growing efforts, which will lead to a greatly improved curative effect on tumor.

With continual achievements of the multicolor PL and high QY, CDs will become more and more promising for optoelectronic applications. For instance, the performance of WLEDs such as CRI and luminous efficiency will be greatly improved by using CDs with high QY as phosphors. For the EL devices, optimization of the charge injection (holes and electrons) with better controlled device fabrication will be further pursed to improve the performance of CDs-based electroluminescent LEDs. The fluorescence of most reported CDs is dominated by surface-defects or molecular states, which fundamentally limits the effectiveness of carrier injection for CDs-based electroluminescent LEDs. The best approach to realizing high performance CDs-based electroluminescent LEDs is to achieve CDs with high-quality bandgap emissions, which has so far remained a challenge. In addition, fluorescent CDs with a narrow full width at half maximum (FWHM < 40 nm) and high color purity comparable to Cd^{2+}/Pb^{2+}-based semiconductor QDs need to be developed for fabricating high performance monochrome LEDs to incubate display technology. For solar energy conversion applications, we foresee that hybrid nanostructures and composites derived from CDs provide a promising platform, and significant advances that tap the potential of such composites in high yield water-splitting and selective CO_2 reduction can be expected. Finally, the newly discovered chiroptical properties of CDs will certainly undergo studies, which may find exciting applications as well in biomedicine and polarization-based optoelectronics in the future.

Acknowledgements

This work was supported by NSFC (21573019), the Major Research Plan of NSFC (21233003), the Fundamental Research Funds for the Central Universities, Key Laboratory of Theoretical and Computational Photochemistry and RGC of Hong Kong (GRF No. 16300915).

References

[1] Y.P. Sun, B. Zhou, Y. Lin, W. Wang, K.A.S. Fernando, P. Pathak, et al., J. Am. Chem. Soc. 128 (2006) 7756.
[2] L.A. Ponomarenko, F. Schedin, M.I. Katsnelson, R. Yang, E.W. Hill, K.S. Novoselov, et al., Science 320 (2008) 356.
[3] C. Ding, A. Zhu, Y. Tian, Acc. Chem. Res. 47 (2014) 20.
[4] K.A.S. Fernando, S. Sahu, Y. Liu, W.K. Lewis, E.A. Guliants, A. Jafariyan, et al., ACS Appl. Mater. Interfaces 7 (2015) 8363.
[5] B. Kong, A. Zhu, C. Ding, X. Zhao, B. Li, Y. Tian, Adv. Mater. 24 (2012) 5844.
[6] Q. Liu, B. Guo, Z. Rao, B. Zhang, J.R. Gong, Nano Lett. 13 (2013) 2436.
[7] S.N. Baker, G.A. Baker, Angew. Chem. Int. Ed. 49 (2010) 6726.
[8] H. Li, Z. Kang, Y. Liu, S.-T. Lee, J. Mater. Chem. 22 (2012) 24230.
[9] Y. Dong, J. Cai, X. You, Y. Chi, Analyst 140 (2015) 7468.
[10] Y. Dong, G. Li, N. Zhou, R. Wang, Y. Chi, G. Chen, Anal. Chem. 84 (2012) 8378.
[11] L. Zhang, Z.-Y. Zhang, R.-P. Liang, Y.-H. Li, J.-D. Qiu, Anal. Chem. 86 (2014) 4423.
[12] S. Li, Y. Li, J. Cao, J. Zhu, L. Fan, X. Li, Anal. Chem. 86 (2014) 10201.
[13] Z. Fan, S. Li, F. Yuan, L. Fan, RSC Adv. 5 (2015) 19773.
[14] Y. Song, S. Zhu, B. Yang, RSC Adv. 4 (2014) 27184.
[15] X.T. Zheng, A. Ananthanarayanan, K.Q. Luo, P. Chen, Small 11 (2015) 1620.
[16] Z. Zhang, J. Zhang, N. Chen, L. Qu, Energy Environ. Sci. 5 (2012) 8869.
[17] J. Liu, Y. Liu, N. Liu, Y. Han, X. Zhang, H. Huang, et al., Science 347 (2015) 970.
[18] S. Zhuo, M. Shao, S.-T. Lee, ACS Nano 6 (2012) 1059.
[19] Y. Li, Y. Zhao, H. Cheng, Y. Hu, G. Shi, L. Dai, et al., J. Am. Chem. Soc. 134 (2011) 15.
[20] Q. Li, S. Zhang, L. Dai, L.-S. Li, J. Am. Chem. Soc. 134 (2012) 18932.
[21] H. Jin, H. Huang, Y. He, X. Feng, S. Wang, L. Dai, et al., J. Am. Chem. Soc. 137 (2015) 7588.
[22] S. Zhu, Q. Meng, L. Wang, J. Zhang, Y. Song, H. Jin, et al., Angew. Chem. Int. Ed. 52 (2013) 4045.
[23] S.M. Sharker, S.M. Kim, S.H. Kim, I. In, H. Lee, S.Y. Park, J. Mater. Chem. B 3 (2015) 5833.
[24] J. Ge, M. Lan, B. Zhou, W. Liu, L. Guo, H. Wang, et al., Nat. Commun. 5 (2014) 4596.
[25] X. Li, Y. Liu, X. Song, H. Wang, H. Gu, H. Zeng, Angew. Chem. Int. Ed. 54 (2015) 1759.
[26] Z. Zhu, J. Ma, Z. Wang, C. Mu, Z. Fan, L. Du, et al., J. Am. Chem. Soc. 136 (2014) 3760.
[27] F. Yuan, L. Ding, Y. Li, X. Li, L. Fan, S. Zhou, et al., Nanoscale 7 (2015) 11727.
[28] M. Zhang, L.L. Bai, W.H. Shang, W.J. Xie, H. Ma, Y.Y. Fu, et al., J. Mater. Chem. 22 (2012) 7461.
[29] X.Y. Tan, Y.C. Li, X.H. Li, S.X. Zhou, L.Z. Fan, S.H. Yang, Chem. Commun. 51 (2015) 2544.
[30] L. Cao, M.J. Meziani, S. Sahu, Y.-P. Sun, Acc. Chem. Res. 46 (2012) 171.
[31] X. Li, M. Rui, J. Song, Z. Shen, H. Zeng, Adv. Funct. Mater. 25 (2015) 4929.
[32] Z. Wang, H. Zeng, L. Sun, J. Mater. Chem. C 3 (2015) 1157.
[33] S.Y. Lim, W. Shen, Z. Gao, Chem. Soc. Rev. 44 (2015) 362.
[34] J. Shen, Y. Zhu, X. Yang, C. Li, Chem. Commun. 48 (2012) 3686.
[35] H. Sun, L. Wu, W. Wei, X. Qu, Mater. Today 16 (2013) 433.
[36] S. Zhu, Y. Song, J. Shao, X. Zhao, B. Yang, Angew. Chem. Int. Ed. 54 (2015) 14626.
[37] M. Vazquez-Nakagawa, L. Rodriguez-Perez, M.A. Herranz, N. Martin, Chem. Commun. 52 (2016) 665.
[38] R. Guo, S. Zhou, Y. Li, X. Li, L. Fan, N.H. Voelcker, ACS Appl. Mater. Interfaces 7 (2015) 23958.
[39] H. Shi, J. Wei, L. Qiang, X. Chen, X. Meng, J. Biomed. Nanotechnol. 10 (2014) 2677.
[40] R. Liu, D. Wu, X. Feng, K. Müllen, J. Am. Chem. Soc. 133 (2011) 15221.
[41] S.C. Ray, A. Saha, N.R. Jana, R. Sarkar, J. Phys. Chem. C 113 (2009) 18546.
[42] X. Li, S. Zhang, S.A. Kulinich, Y. Liu, H. Zeng, Sci. Rep. 4 (2014) 4976.
[43] B. Mandal, S. Sarkar, P. Sarkar, J. Nanopart. Res. 14 (2012) 1317.
[44] Y. Li, H. Shu, X. Niu, J. Wang, J. Phys. Chem. C 119 (2015) 24950.
[45] S.S.R.K.C. Yamijala, A. Bandyopadhyay, S.K. Pati, J. Phys. Chem. C 117 (2013) 23295.
[46] J. Guettinger, C. Stampfer, T. Frey, T. Ihn, K. Ensslin, Phys. Status Solidi B 246 (2009) 2553.
[47] X. Li, S.P. Lau, L. Tang, R. Ji, P. Yang, Nanoscale 6 (2014) 5323.
[48] M. Bottini, C. Balasubramanian, M.I. Dawson, A. Bergamaschi, S. Bellucci, T. Mustelin, J. Phys. Chem. B 110 (2006) 831.
[49] V. Nguyen, J. Si, L. Yan, X. Hou, Carbon 95 (2015) 659.
[50] J. Lee, K. Kim, W.I. Park, B.-H. Kim, J.H. Park, T.-H. Kim, et al., Nano Lett. 12 (2012) 6078.
[51] L. Fan, M. Zhu, X. Lee, R. Zhang, K. Wang, J. Wei, et al., Part. Part. Syst. Charact. 30 (2013) 764.
[52] Z.T. Fan, Y.C. Li, X.H. Li, L.Z. Fan, S.X. Zhou, D.C. Fang, et al., Carbon 70 (2014) 149.
[53] Y. Li, Y. Hu, Y. Zhao, G. Shi, L. Deng, Y. Hou, et al., Adv. Mater. 23 (2011) 776.
[54] T.F. Li, Y.W. Li, L. Xiao, H.T. Yu, L.Z. Fan, Acta Chim. Sinica 72 (2014) 227.
[55] A. Ananthanarayanan, X.W. Wang, P. Routh, B. Sana, S. Lim, D.H. Kim, et al., Adv. Funct. Mater. 24 (2014) 3021.
[56] D.B. Shinde, V.K. Pillai, Angew. Chem. Int. Ed. 52 (2013) 2542.
[57] D. Pan, J. Zhang, Z. Li, M. Wu, Adv. Mater. 22 (2010) 734.
[58] D. Pan, L. Guo, J. Zhang, C. Xi, Q. Xue, H. Huang, et al., J. Mater. Chem. 22 (2012) 3314.
[59] H. Tetsuka, R. Asahi, A. Nagoya, K. Okamoto, I. Tajima, R. Ohta, et al., Adv. Mater. 24 (2012) 5333.
[60] S. Chen, J.-W. Liu, M.-L. Chen, X.-W. Chen, J.-H. Wang, Chem. Commun. 48 (2012) 7637.
[61] L.-L. Li, J. Ji, R. Fei, C.-Z. Wang, Q. Lu, J.-R. Zhang, et al., Adv. Funct. Mater. 22 (2012) 2971.
[62] F. Liu, M.-H. Jang, H.D. Ha, J.-H. Kim, Y.-H. Cho, T.S. Seo, Adv. Mater. 25 (2013) 3657.

[63] L. Lin, S. Zhang, Chem. Commun. 48 (2012) 10177.
[64] X. Zhou, Y. Zhang, C. Wang, X. Wu, Y. Yang, B. Zheng, et al., ACS Nano 6 (2012) 6592.
[65] Y. Dong, C. Chen, X. Zheng, L. Gao, Z. Cui, H. Yang, et al., J. Mater. Chem. 22 (2012) 8764.
[66] J. Peng, W. Gao, B.K. Gupta, Z. Liu, R. Romero-Aburto, L. Ge, et al., Nano Lett. 12 (2012) 844.
[67] R. Ye, C. Xiang, J. Lin, Z. Peng, K. Huang, Z. Yan, et al., Nat. Commun. 4 (2013) 2943.
[68] H. Yu, X. Li, X. Zeng, Y. Lu, Chem. Commun. 52 (2016) 819.
[69] Y. Dong, H. Pang, H.B. Yang, C. Guo, J. Shao, Y. Chi, et al., Angew. Chem. Int. Ed. 52 (2013) 7800.
[70] Z. Huang, Y. Shen, Y. Li, W. Zheng, Y. Xue, C. Qin, et al., Nanoscale 6 (2014) 13043.
[71] X. Yan, X. Cui, L.-S. Li, J. Am. Chem. Soc. 132 (2010) 5944.
[72] L. Wang, Y. Wang, T. Xu, H. Liao, C. Yao, Y. Liu, et al., Nat. Commun. 5 (2014) 5357.
[73] Y.Q. Dong, J.W. Shao, C.Q. Chen, H. Li, R.X. Wang, Y.W. Chi, et al., Carbon 50 (2012) 4738.
[74] L. Tang, R. Ji, X. Cao, J. Lin, H. Jiang, X. Li, et al., ACS Nano 6 (2012) 5102.
[75] X. Wu, F. Tian, W. Wang, J. Chen, M. Wu, J.X. Zhao, J. Mater. Chem. C 1 (2013) 4676.
[76] C.-W. Lai, Y.-H. Hsiao, Y.-K. Peng, P.-T. Chou, J. Mater. Chem. 22 (2012) 14403.
[77] C. Liu, P. Zhang, X. Zhai, F. Tian, W. Li, J. Yang, et al., Biomaterials 33 (2012) 3604.
[78] X. Jia, J. Li, E. Wang, Nanoscale 4 (2012) 5572.
[79] J. Jiang, Y. He, S. Li, H. Cui, Chem. Commun. 48 (2012) 9634.
[80] S.K. Bhunia, A. Saha, A.R. Maity, S.C. Ray, N.R. Jana, Sci. Rep. 3 (2013) 1473.
[81] L. Tang, R. Ji, X. Li, G. Bai, C.P. Liu, J. Hao, et al., ACS Nano 8 (2014) 6312.
[82] Y. Wang, Y. Li, Y. Yan, J. Xu, B. Guan, Q. Wang, et al., Chem. Commun. 49 (2013) 9006.
[83] X. Wang, K. Qu, B. Xu, J. Ren, X. Qu, Nano Res. 4 (2011) 908.
[84] K.P. Loh, Q. Bao, G. Eda, M. Chhowalla, Nat. Commun. 2 (2010) 1015.
[85] D. Qu, M. Zheng, L. Zhang, H. Zhao, Z. Xie, X. Jing, et al., Sci. Rep. 4 (2014) 5294.
[86] J. Shen, Y. Zhu, X. Yang, J. Zong, J. Zhang, C. Li, New J. Chem. 36 (2012) 97.
[87] X. Wang, L. Cao, S.-T. Yang, F. Lu, M.J. Meziani, L. Tian, et al., Angew. Chem. Int. Ed. 49 (2010) 5310.
[88] J. Shen, Y. Zhu, C. Chen, X. Yang, C. Li, Chem. Commun. 47 (2011) 2580.
[89] S. Zhu, J. Zhang, S. Tang, C. Qiao, L. Wang, H. Wang, et al., Adv. Funct. Mater. 22 (2012) 4732.
[90] J. Zong, Y. Zhu, X. Yang, J. Shen, C. Li, Chem. Commun. 47 (2011) 764.
[91] Z. Gan, X. Wu, G. Zhou, J. Shen, P.K. Chu, Adv. Opt. Mater. 1 (2013) 554.
[92] X. Li, H. Wang, Y. Shimizu, A. Pyatenko, K. Kawaguchi, N. Koshizaki, Chem. Commun. 47 (2011) 932.
[93] S.J. Zhu, J.H. Zhang, C.Y. Qiao, S.J. Tang, Y.F. Li, W.J. Yuan, et al., Chem. Commun. 47 (2011) 6858.
[94] Y. Wang, J. Xu, Y. Wang, H. Chen, Chem. Soc. Rev. 42 (2013) 2930.
[95] C. Tao, L. Jiao, O.V. Yazyev, Y.-C. Chen, J. Feng, X. Zhang, et al., Nat. Phys. 7 (2011) 616.
[96] N. Suzuki, Y. Wang, P. Elvati, Z.-B. Qu, K. Kim, S. Jiang, et al., ACS Nano 10 (2016) 1744.
[97] S. Kim, S.W. Hwang, M.-K. Kim, D.Y. Shin, D.H. Shin, C.O. Kim, et al., ACS Nano 6 (2012) 8203.
[98] S. Zhu, S. Tang, J. Zhang, B. Yang, Chem. Commun. 48 (2012) 4527.
[99] G. Eda, Y.-Y. Lin, C. Mattevi, H. Yamaguchi, H.-A. Chen, I.S. Chen, et al., Adv. Mater. 22 (2010) 505.
[100] M.A. Sk, A. Ananthanarayanan, L. Huang, K.H. Lim, P. Chen, J. Mater. Chem. 2 (2014) 6954.
[101] W. Kwon, Y.-H. Kim, C.-L. Lee, M. Lee, H.C. Choi, T.-W. Lee, et al., Nano Lett. 14 (2014) 1306.
[102] H. Li, X. He, Z. Kang, H. Huang, Y. Liu, J. Liu, et al., Angew. Chem. Int. Ed. 49 (2010) 4532.
[103] K. Jiang, S. Sun, L. Zhang, Y. Lu, A. Wu, C. Cai, et al., Angew. Chem. Int. Ed. 54 (2015) 5360.
[104] A. Nourbakhsh, M. Cantoro, T. Vosch, G. Pourtois, F. Clemente, M.H. van der Veen, et al., Nanotechnology 21 (2010) 435203.
[105] T. Gokus, R.R. Nair, A. Bonetti, M. Boehmler, A. Lombardo, K.S. Novoselov, et al., ACS Nano 3 (2009) 3963.
[106] L. Bao, C. Liu, Z.-L. Zhang, D.-W. Pang, Adv. Mater. 27 (2015) 1663.
[107] L. Bao, Z.-L. Zhang, Z.-Q. Tian, L. Zhang, C. Liu, Y. Lin, et al., Adv. Mater. 23 (2011) 5801.
[108] C.-T. Chien, S.-S. Li, W.-J. Lai, Y.-C. Yeh, H.-A. Chen, I.S. Chen, et al., Angew. Chem. Int. Ed. 51 (2012) 6662.
[109] M.X. Gao, C.F. Liu, Z.L. Wu, Q.L. Zeng, X.X. Yang, W.B. Wu, et al., Chem. Commun. 49 (2013) 8015.
[110] S. Hu, A. Trinchi, P. Atkin, I. Cole, Angew. Chem. Int. Ed. 54 (2015) 2970.
[111] H. Ding, S.-B. Yu, J.-S. Wei, H.-M. Xiong, ACS Nano 10 (2016) 484.
[112] Y. Liu, C.-Y. Liu, Z.-Y. Zhang, J. Mater. Chem. C 1 (2013) 4902.
[113] L. Wang, S.-J. Zhu, H.-Y. Wang, S.-N. Qu, Y.-L. Zhang, J.-H. Zhang, et al., ACS Nano 8 (2014) 2541.
[114] W. Zhao, C.H. Song, P.E. Pehrsson, J. Am. Chem. Soc. 124 (2002) 12418.
[115] S.H. Jin, D.H. Kim, G.H. Jun, S.H. Hong, S. Jeon, ACS Nano 7 (2012) 1239.
[116] G.S. Kumar, R. Roy, D. Sen, U.K. Ghorai, R. Thapa, N. Mazumder, et al., Nanoscale 6 (2014) 3384.
[117] L. Guo, J. Ge, W. Liu, G. Niu, Q. Jia, H. Wang, et al., Nanoscale 8 (2016) 729.
[118] L. Wang, S.-J. Zhu, H.-Y. Wang, Y.-F. Wang, Y.-W. Hao, J.-H. Zhang, et al., Adv. Opt. Mater. 1 (2013) 264.
[119] V. Gupta, N. Chaudhary, R. Srivastava, G.D. Sharma, R. Bhardwaj, S. Chand, J. Am. Chem. Soc. 133 (2011) 9960.
[120] X. Wang, L. Cao, F. Lu, M.J. Meziani, H. Li, G. Qi, et al., Chem. Commun. (2009) 3774.
[121] K.J. Williams, C.A. Nelson, X. Yan, L.-S. Li, X. Zhu, ACS Nano 7 (2013) 1388.
[122] M.L. Mueller, X. Yan, J.A. McGuire, L.-S. Li, Nano Lett. 10 (2010) 2679.
[123] M.L. Mueller, X. Yan, B. Dragnea, L.-S. Li, Nano Lett. 11 (2011) 56.
[124] Y. Zhao, Q. Liu, S. Shakoor, J.R. Gong, D. Wang, Toxicol. Res. 4 (2015) 270.
[125] M. Havrdova, K. Hola, J. Skopalik, K. Tomankova, M. Petr, K. Cepe, et al., Carbon 99 (2016) 238.
[126] M. Nurunnabi, Z. Khatun, K.M. Huh, S.Y. Park, D.Y. Lee, K.J. Cho, et al., ACS Nano 7 (2013) 6858.
[127] N. Parvin, T.K. Mandal, RSC Adv. 6 (2016) 18134.
[128] D.J. Prockop, Science 293 (2001) 211.
[129] G.C. Parker, M. Anastassova-Kristeva, L.M. Eisenberg, M.S. Rao, M.A. Williams, P.R. Sanberg, et al., Stem Cells Dev. 14 (2005) 463.
[130] K. Jiang, S. Sun, L. Zhang, Y. Wang, C. Cai, H. Lin, ACS Appl. Mater. Interfaces 7 (2015) 23231.
[131] H.K. Sadhanala, K.K. Nanda, Carbon 96 (2016) 166.
[132] W. Dong, S. Zhou, Y. Dong, J. Wang, X. Ge, L. Sui, Luminescence 30 (2015) 867.
[133] L. Shi, Y. Li, X. Li, X. Wen, G. Zhang, J. Yang, et al., Nanoscale 7 (2015) 7394.
[134] W. Shang, X. Zhang, M. Zhang, Z. Fan, Y. Sun, M. Han, et al., Nanoscale 6 (2014) 5799.
[135] Y.E.L. Bai, L. Fan, M. Han, X. Zhang, S. Yang, J. Mater. Chem. 21 (2011) 819.
[136] C. Wang, Y.E.L. Fan, Z. Wang, H. Liu, Y. Li, et al., Adv. Mater. 19 (2007) 3677.
[137] J.-H. Liu, L. Cao, G.E. LeCroy, P. Wang, M.J. Meziani, Y. Dong, et al., ACS Appl. Mater. Interfaces 7 (2015) 19439.
[138] Z. Yu, T.G. Pestell, M.P. Lisanti, R.G. Pestell, Int. J. Biochem. Cell Biol. 44 (2012) 2144.
[139] Q. Bao, Y. Zhao, A. Renner, H. Niess, H. Seeliger, K.-W. Jauch, et al., Cancers 2 (2010) 1629.
[140] T. Reya, S.J. Morrison, M.F. Clarke, I.L. Weissman, Nature 414 (2001) 105.
[141] C. Li, Y. Liu, Y. Wu, Y. Sun, F. Li, Biomaterials 34 (2013) 1223.
[142] R.W. Horobin, J.C. Stockert, F. Rashid-Doubell, Histochem. Cell Biol. 139 (2013) 623.
[143] K.K.R. Datta, O. Kozak, V. Ranc, M. Havrdova, A.B. Bourlinos, K. Safarova, et al., Chem. Commun. 50 (2014) 10782.
[144] Y.-F. Kang, Y.-W. Fang, Y.-H. Li, W. Li, X.-B. Yin, Chem. Commun. 51 (2015) 16956.
[145] H. Wang, X. Wang, RSC Adv. 5 (2015) 75380.
[146] L. Cao, X. Wang, M.J. Meziani, F. Lu, H. Wang, P.G. Luo, et al., J. Am. Chem. Soc. 129 (2007) 11318.
[147] Y. Hu, J. Yang, J. Tian, L. Jia, J.-S. Yu, RSC Adv. 5 (2015) 15366.
[148] G. Tong, J. Wang, R. Wang, X. Guo, L. He, F. Qiu, et al., J. Mater. Chem. B 3 (2015) 700.
[149] J. Ge, Q. Jia, W. Liu, L. Guo, Q. Liu, M. Lan, et al., Adv. Mater. 27 (2015) 4169.
[150] Y. Wang, Y. Meng, S. Wang, C. Li, W. Shi, J. Chen, et al., Small 11 (2015) 3575.
[151] S. Ruan, J. Qian, S. Shen, J. Zhu, X. Jiang, Q. He, et al., Nanoscale 6 (2014) 10040.
[152] J.A. Barreto, W. O'Malley, M. Kubeil, B. Graham, H. Stephan, L. Spiccia, Adv. Mater. 23 (2011) H18.
[153] Y. Liu, J.-J. Yin, Z. Nie, Nano Res. 7 (2014) 1719.
[154] I.L. Christensen, Y.-P. Sun, P. Juzenas, J. Biomed. Nanotechnol. 7 (2011) 667.
[155] Z.M. Markovic, B.Z. Ristic, K.M. Arsikin, D.G. Klisic, L.M. Harhaji-Trajkovic, B.M. Todorovic-Markovic, et al., Biomaterials 33 (2012) 7084.
[156] P. Agostinis, K. Berg, K.A. Cengel, T.H. Foster, A.W. Girotti, S.O. Gollnick, et al., CA Cancer. J. Clin. 61 (2011) 250.
[157] J. Ge, Q. Jia, W. Liu, M. Lan, B. Zhou, L. Guo, et al., Adv. Healthc. Mater. 5 (2016) 665.
[158] J.P. Celli, B.Q. Spring, I. Rizvi, C.L. Evans, K.S. Samkoe, S. Verma, et al., Chem. Rev. 110 (2010) 2795.
[159] M. Hockel, P. Vaupel, J. Natl. Cancer Inst. 93 (2001) 266.
[160] Y. Sun, S. Wang, C. Li, P. Luo, L. Tao, Y. Wei, et al., Phys. Chem. Chem. Phys. 15 (2013) 9907.
[161] B.W. Henderson, T.J. Dougherty, Photochem. Photobiol. 55 (1992) 145.
[162] B.W. Henderson, V.H. Fingar, Cancer Res. 47 (1987) 3110.
[163] A.L. Maas, S.L. Carter, E.P. Wileyto, J. Miller, M. Yuan, G. Yu, et al., Cancer Res. 72 (2012) 2079.
[164] E.B. Caruso, S. Petralia, S. Conoci, S. Giuffrida, S. Sortino, J. Am. Chem. Soc. 129 (2007) 480.
[165] P.N. Coneski, M.H. Schoenfisch, Chem. Soc. Rev. 41 (2012) 3753.
[166] D.A. Riccio, M.H. Schoenfisch, Chem. Soc. Rev. 41 (2012) 3731.
[167] A.B. Seabra, N. Duran, J. Mater. Chem. 20 (2010) 1624.
[168] J. Xu, F. Zeng, H. Wu, S. Wu, J. Mater. Chem. B 3 (2015) 4904.
[169] A.M. Smith, M.C. Mancini, S. Nie, Nat. Nanotechnol. 4 (2009) 710.
[170] C. Fowley, A.P. McHale, B. McCaughan, A. Fraix, S. Sortino, J.F. Callan, Chem. Commun. 51 (2015) 81.
[171] K. Hola, Y. Zhang, Y. Wang, E.P. Giannelis, R. Zboril, A.L. Rogach, Nano Today 9 (2014) 590.
[172] C.-B. Ma, Z.-T. Zhu, H.-X. Wang, X. Huang, X. Zhang, X. Qi, et al., Nanoscale 7 (2015) 10162.
[173] J. Kim, J. Park, H. Kim, K. Singha, W.J. Kim, Biomaterials 34 (2013) 7168.
[174] L. Hu, Y. Sun, S. Li, X. Wang, K. Hu, L. Wang, et al., Carbon 67 (2014) 508.

[175] P. Pierrat, R. Wang, D. Kereselidze, M. Lux, P. Didier, A. Kichler, et al., Biomaterials 51 (2015) 290.
[176] L. Cheng, Y. Li, X. Zhai, B. Xu, Z. Cao, W. Liu, ACS Appl. Mater. Interfaces 6 (2014) 20487.
[177] L. Wang, X. Wang, A. Bhirde, J. Cao, Y. Zeng, X. Huang, et al., Adv. Healthc. Mater. 3 (2014) 1203.
[178] H. Ding, F. Du, P. Liu, Z. Chen, J. Shen, ACS Appl. Mater. Interfaces 7 (2015) 6889.
[179] M.Z. Fahmi, J.-K. Chen, C.-C. Huang, Y.-C. Ling, J.-Y. Chang, J. Mater. Chem. B 3 (2015) 5532.
[180] Y.K. Jung, E. Shin, B.-S. Kim, Sci. Rep. 5 (2015) 18807.
[181] I. Matai, A. Sachdev, P. Gopinath, ACS Appl. Mater. Interfaces 7 (2015) 11423.
[182] J. Qiu, R. Zhang, J. Li, Y. Sang, W. Tang, P.R. Gil, et al., Int. J. Nanomed. 10 (2015) 6709.
[183] J. Tang, B. Kong, H. Wu, M. Xu, Y. Wang, Y. Wang, et al., Adv. Mater. 25 (2013) 6569.
[184] C. Wang, C. Wu, X. Zhou, T. Han, X. Xin, J. Wu, et al., Sci. Rep. 3 (2013) 1542.
[185] H. Wang, Y. Sun, J. Yi, J. Fu, J. Di, A.D.C. Alonso, et al., Biomaterials 53 (2015) 117.
[186] S. Beack, W.H. Kong, H.S. Jung, I.H. Do, S. Han, H. Kim, et al., Acta Biomater. 26 (2015) 295.
[187] Y. Choi, S. Kim, M.-H. Choi, S.-R. Ryoo, J. Park, D.-H. Min, et al., Adv. Funct. Mater. 24 (2014) 5781.
[188] C. Fowley, N. Nomikou, A.P. McHale, B. McCaughan, J.F. Callan, Chem. Commun. 49 (2013) 8934.
[189] J. Wang, Z. Zhang, S. Zha, Y. Zhu, P. Wu, B. Ehrenberg, et al., Biomaterials 35 (2014) 9372.
[190] L. Zhou, X. Ge, J. Zhou, S. Wei, J. Shen, Chem. Commun. 51 (2015) 421.
[191] P. Huang, J. Lin, X. Wang, Z. Wang, C. Zhang, M. He, et al., Adv. Mater. 24 (2012) 5104.
[192] M. Zheng, S. Liu, J. Li, D. Qu, H. Zhao, X. Guan, et al., Adv. Mater. 26 (2014) 3554.
[193] C.P. Leamon, P.S. Low, Drug Discov. Today 6 (2001) 44.
[194] A. Doering, W. Birnbaum, D. Kuckling, Chem. Soc. Rev. 42 (2013) 7391.
[195] J. Gao, H. Gu, B. Xu, Acc. Chem. Res. 42 (2009) 1097.
[196] D. Shi, Adv. Funct. Mater. 19 (2009) 3356.
[197] H. Wang, G. Cao, Z. Gai, K. Hong, P. Banerjee, S. Zhou, Nanoscale 7 (2015) 7885.
[198] H. Wang, J. Di, Y. Sun, J. Fu, Z. Wei, H. Matsui, et al., Adv. Funct. Mater. 25 (2015) 5537.
[199] H. Wang, J. Yi, S. Mukherjee, P. Banerjee, S. Zhou, Nanoscale 6 (2014) 13001.
[200] J. Kwak, W.K. Bae, D. Lee, I. Park, J. Lim, M. Park, et al., Nano Lett. 12 (2012) 2362.
[201] Q. Sun, Y.A. Wang, L.S. Li, D. Wang, T. Zhu, J. Xu, et al., Nat. Photonics 1 (2007) 717.
[202] X.T. Feng, F. Zhang, Y.L. Wang, Y. Zhang, Y.Z. Yang, X.G. Liu, Appl. Phys. Lett. 107 (2015) 213102.
[203] L.-H. Mao, W.-Q. Tang, Z.-Y. Deng, S.-S. Liu, C.-F. Wang, S. Chen, Ind. Eng. Chem. Res 53 (2014) 6417.
[204] C. Shen, J. Wang, Y. Cao, Y. Lu, J. Mater. Chem. C 3 (2015) 6668.
[205] M. Sun, S. Qu, Z. Hao, W. Ji, P. Jing, H. Zhang, et al., Nanoscale 6 (2014) 13076.
[206] H. Tetsuka, A. Nagoya, R. Asahi, J. Mater. Chem. C 3 (2015) 3536.
[207] W. Zhang, S.F. Yu, L. Fei, L. Jin, S. Pan, P. Lin, Carbon 85 (2015) 344.
[208] P.K. Sarswat, M.L. Free, Phys. Chem. Chem. Phys. 17 (2015) 27642.
[209] L. Chen, C. Zhang, Z. Du, H. Li, L. Zhang, W. Zou, Macromol. Mater. Eng. 300 (2015) 1232.
[210] L. Chen, C. Zhang, Z. Du, H. Li, L. Zhang, W. Zou, J. Appl. Polym. Sci. 132 (2015).
[211] L. Ma, W. Xiang, H. Gao, L. Pei, X. Ma, Y. Huang, et al., J. Mater. Chem. C 3 (2015) 6764.
[212] X. Guo, C.-F. Wang, Z.-Y. Yu, L. Chen, S. Chen, Chem. Commun. 48 (2012) 2692.
[213] Q.-L. Chen, C.-F. Wang, S. Chen, J. Mater. Sci. 48 (2013) 2352.
[214] W. Kwon, S. Do, J. Lee, S. Hwang, J.K. Kim, S.-W. Rhee, Chem. Mater. 25 (2013) 1893.
[215] C. Sun, Y. Zhang, Y. Wang, W. Liu, S. Kalytchuk, S.V. Kershaw, et al., Appl. Phys. Lett. 104 (2014) 261106.
[216] C. Sun, Y. Zhang, K. Sun, C. Reckmeier, T. Zhang, X. Zhang, et al., Nanoscale 7 (2015) 12045.
[217] Y. Chen, M. Zheng, Y. Xiao, H. Dong, H. Zhang, J. Zhuang, et al., Adv. Mater. 28 (2016) 312.
[218] W. Kwon, S. Do, J.-H. Kim, M.S. Jeong, S.-W. Rhee, Sci. Rep. 5 (2015) 12604.
[219] F. Wang, Y.-H. Chen, C.-Y. Liu, D.-G. Ma, Chem. Commun. 47 (2011) 3502.
[220] X. Zhang, Y. Zhang, Y. Wang, S. Kalytchuk, S.V. Kershaw, Y. Wang, et al., ACS Nano 7 (2013) 11234.
[221] J.K. Kim, S. Bae, Y. Yi, M.J. Park, S.J. Kim, N. Myoung, et al., Sci. Rep. 5 (2015) 11032.
[222] X. Li, Y. Wu, S. Zhang, B. Cai, Y. Gu, J. Song, et al., Adv. Funct. Mater. 26 (2016) 2435.
[223] J. Song, J. Li, X. Li, L. Xu, Y. Dong, H. Zeng, Adv. Mater. 27 (2015) 7162.
[224] Y. Wang, X. Li, J. Song, L. Xiao, H. Zeng, H. Sun, Adv. Mater. 27 (2015) 7101.
[225] P. Mirtchev, E.J. Henderson, N. Soheilnia, C.M. Yip, G.A. Ozin, J. Mater. Chem. 22 (2012) 1265.
[226] X. Fang, M. Li, K. Guo, J. Li, M. Pan, L. Bai, et al., Electrochim. Acta 137 (2014) 634.
[227] C. Xie, B. Nie, L. Zeng, F.-X. Liang, M.-Z. Wang, L. Luo, et al., ACS Nano 8 (2014) 4015.
[228] P. Gao, K. Ding, Y. Wang, K. Ruan, S. Diao, Q. Zhang, et al., J. Phys. Chem. C 118 (2014) 5164.
[229] I. Mihalache, A. Radoi, M. Mihaila, C. Munteanu, A. Marin, M. Danila, et al., Electrochim. Acta 153 (2015) 306.
[230] C. Liu, K. Chang, W. Guo, H. Li, L. Shen, W. Chen, et al., Appl. Phys. Lett. 105 (2014) 073306.
[231] J.J. Huang, Z.F. Zhong, M.Z. Rong, X. Zhou, X.D. Chen, M.Q. Zhang, Carbon 70 (2014) 190.
[232] L. Cao, S. Sahu, P. Anilkumar, C.E. Bunker, J. Xu, K.A.S. Fernando, et al., J. Am. Chem. Soc. 133 (2011) 4754.
[233] H. Yu, Y. Zhao, C. Zhou, L. Shang, Y. Peng, Y. Cao, et al., J. Mater. Chem. A 2 (2014) 3344.
[234] X. Zhang, F. Wang, H. Huang, H. Li, X. Han, Y. Liu, et al., Nanoscale 5 (2013) 2274.
[235] S. Xie, H. Su, W. Wei, M. Li, Y. Tong, Z. Mao, J. Mater. Chem. A 2 (2014) 16365.
[236] J. Wang, Y.-F. Lim, G.W. Hoa, Nanoscale 6 (2014) 9673.
[237] Y.-X. Qi, M. Zhang, Q.-Q. Fu, R. Liu, G.-Y. Shi, Chem. Commun. 49 (2013) 10599.
[238] J. Liu, H. Zhang, D. Tang, X. Zhang, L. Yan, Y. Han, et al., ChemCatChem 6 (2014) 2634.
[239] J. Hou, H. Cheng, C. Yang, O. Takeda, H. Zhu, Nano Energy 18 (2015) 143.
[240] B.C.M. Martindale, G.A.M. Hutton, C.A. Caputo, E. Reisner, J. Am. Chem. Soc. 137 (2015) 6018.
[241] M. Li, R. Zhao, Y. Su, Z. Yang, Y. Zhang, Nanoscale 8 (2016) 8559.
[242] F. Nan, Z. Kang, J. Wang, M. Shen, L. Fang, Appl. Phys. Lett. 106 (2015) 153901.
[243] T.-F. Yeh, C.-Y. Teng, S.-J. Chen, H. Teng, Adv. Mater. 26 (2014) 3297.

Fanglong Yuan obtained his BS degree in Applied Chemistry in Beijing University of Chemical Technology in 2013. He is now a Ph.D. student under the supervision of Prof. Louzhen Fan at Beijing Normal University. His research interests are centered on the synthesis and optoelectronic applications of fluorescent carbon nanomaterials.

Shuhua Li obtained her Master's degree in physical chemistry from Beijing Normal University in 2015. Currently, she is a Ph.D. student under the supervision of Prof. Louzhen Fan at Beijing Normal University. Her research interests focus on fluorescent carbon nanomaterials for biomedical applications.

Zetan Fan received her Ph.D. in physical chemistry in 2016 under the supervision of Prof. Louzhen Fan at Beijing Normal University. After graduation, she will go to The Hong Kong Polytechnic University working as a postdoctoral fellow. Her research interests focus on preparation and function of carbon nanomaterials for biological applications.

Xiangyue Meng received his Ph.D. from Institute of Chemistry Chinese Academy of Sciences in 2014. Now, he is visiting Scholar in the Hong Kong University of Science and Technology (with Prof. Shihe Yang). Since 2014, he has been associate professor at Beijing University of Chemical Technology. His main research activities focus on the development of organic functional materials for various optoelectronic applications.

Louzhen Fan is now a chemistry professor of Department of Chemistry, Beijing Normal University. She received her Ph.D. in physical chemistry in 1998 under the supervision of Prof. Daoben Zhu and Prof. Yongfang Li from Institute of Chemistry, the Chinese Academy of Sciences, Beijing. Her research interests are focused on the synthesis of novel carbon and metal nanomaterials and their applications in biology and energy.

Shihe Yang received his B.S. in Polymer Chemistry from Sun Yat-Sen University in China and Ph.D. in Physical Chemistry from Rice University (with Prof. Richard E. Smalley). He did post-doctoral research at Argonne National Laboratory and the University of Toronto (with Prof. John C. Polanyi) before joining the faculty at The Hong Kong University of Science and Technology, where he is currently a full Professor. He has long engaged in the studies on the chemistry and physics of clusters, fullerenes and nanomaterials. His current research interest is focused on energy material science, technology and physical chemistry by drawing on the understanding, manipulation and applications of low-dimensional nanosystems, materials and interfaces.